Tango1 spatially organizes ER exit sites to control ER export

Min Liu,* Zhi Feng,* Hongmei Ke, Ying Liu, Tianhui Sun, Jianli Dai, Wenhong Cui, and José Carlos Pastor-Pareja

School of Life Sciences, Tsinghua University, Beijing 100084, China

Exit of secretory cargo from the endoplasmic reticulum (ER) takes place at specialized domains called ER exit sites (ERESs). In mammals, loss of TANGO1 and other MIA/cTAGE (melanoma inhibitory activity/cutaneous T cell lymphoma–associated antigen) family proteins prevents ER exit of large cargoes such as collagen. Here, we show that *Drosophila melanogaster* Tango1, the only MIA/cTAGE family member in fruit flies, is a critical organizer of the ERES–Golgi interface. Tango1 rings hold COPII (coat protein II) carriers and Golgi in close proximity at their center. Loss of Tango1, present at ERESs in all tissues, reduces ERES size and causes ERES–Golgi uncoupling, which impairs secretion of not only collagen, but also all other cargoes we examined. Further supporting an organizing role of Tango1, its overexpression creates more and larger ERESs. Our results suggest that spatial coordination of ERES, carrier, and Golgi elements through Tango1's multiple interactions increases secretory capacity in *Drosophila* and allows secretion of large cargo.

Introduction

Secreted proteins reach the extracellular space through a controlled series of membrane traffic events ensuring fusion of cargo-containing secretory vesicles with the plasma membrane (Bonifacino and Glick, 2004). After translocation into the ER, secretory cargo is collected at specialized cup-shaped regions of the ER and then loaded into membrane vesicles that transfer the cargo to the Golgi compartment (Bannykh et al., 1996). These specialized regions of the ER are known as ER exit sites (ERESs) or transitional ER, the latter emphasizing their dynamic relation with the Golgi. At the ERES, vesicles budding from the ER in the direction of the Golgi are generated by the coat protein II (COPII) complex, a set of proteins highly conserved in all eukaryotes (Jensen and Schekman, 2011). Structural studies have shown that budding of COPII vesicles from ERES is mediated by the assembly of a vesicle-enclosing cage of 60–90 nm in diameter, yet many secreted proteins exceed the dimensions of this cage and are efficiently secreted by cells, raising the question of how this happens (Fromme and Schekman, 2005; Miller and Schekman, 2013). Examples of large secreted proteins include collagens, the main component of extracellular matrices in all animals, for which trimers assemble in the ER into long semirigid rods (Canty and Kadler, 2005).

TANGO1, a protein belonging to the MIA/cTAGE family (melanoma inhibitory activity/cutaneous T cell lymphoma–associated antigen; Usener et al., 2003; Malhotra and Erlmann, 2011), has been shown to be involved in the transport of collagens from the ERES to Golgi. Tango1 was discovered in a screening for genes affecting secretion in *Drosophila melanogaster* S2 cells (Bard et al., 2006) and confirmed in a second similar screening (Wendler et al., 2010). It was later found that human TANGO1 was required for the secretion of collagen but not other secreted proteins (Saito et al., 2009). This was supported by a TANGO1 knockout mutant mouse which indeed showed defects in the deposition of multiple types of collagens (Wilson et al., 2011). TANGO1 is a transmembrane protein localized specifically at ERES. The luminal portion of TANGO1 contains an SH3-like domain at its N terminus that is capable of binding collagen at the ER lumen (Saito et al., 2009) through the chaperone Hsp49 (Ishikawa et al., 2016). The cytoplasmic portion contains a region with two presumed coiled coils and a Pro-rich region at its C terminus through which TANGO1 may interact with the COPII coat (Saito et al., 2009). It has been proposed that TANGO1 collects collagen at ERESs as a specific receptor while at the same time ensuring that a large enough vesicle is formed to package that cargo. Activities of TANGO1 in both retarding COPII coat assembly and recruiting ER–Golgi intermediate compartment (ERGIC) membranes to nascent vesicles have been proposed as mechanisms by which TANGO1 can mediate formation of such megacarrier vesicles (Malhotra and Erlmann, 2015; Santos et al., 2015).

Apart from TANGO1, the human genome contains additional TANGO1-like proteins of the MIA/cTAGE family. These include a short splice variant of TANGO1 (TANGO1S) and eight other members of the MIA/cTAGE family of proteins (Malhotra and Erlmann, 2011). Common to all these TANGO1-

*M. Liu and Z. Feng contributed equally to this paper.

Correspondence to José Carlos Pastor-Pareja: jose.pastor@biomed.tsinghua.edu.cn

Abbreviations used: ERES, ER exit site; ERGIC, ER–Golgi intermediate compartment; SIM, structured illumination microscopy.

The Rockefeller University Press $30.00
J. Cell Biol. Vol. 216 No. 4 1035–1049
https://doi.org/10.1083/jcb.201611088

like proteins is the presence of transmembrane, coiled-coil and Pro-rich regions highly similar to the cytoplasmic portion of TANGO1. In contrast to full-length TANGO1, however, they lack the SH3-like domain and extended intraluminal region. Nonetheless, a function in secretion has been shown for some of these proteins. TANGO1S, lacking the signal peptide and luminal domain of the full protein but preserving its transmembrane domain, is involved in collagen secretion (Maeda et al., 2016). Also involved in collagen secretion is cTAGE5 (Saito et al., 2011, 2014; Tanabe et al., 2016). Finally, TALI, a chimeric protein resulting from fusion of MIA2 and cTAGE5 gene products, is required for the secretion of ApoB-containing large lipoparticles (Santos et al., 2016).

Besides TANGO1 and TANGO1-like proteins, loss of several factors potentially involved in general secretion have been shown to affect preferentially collagen secretion in mammalian cells. These include the TRAPP tethering complex component Sedlin (Venditti et al., 2012), ubiquitination of Sec31 by the ubiquitin ligase KLHL12 (Jin et al., 2012), Syntaxin 18, and the SNARE regulator Sly1 (Nogueira et al., 2014). Notably, mutations in the Sec23A subunit of COPII led to craniofacial development defects attributable to aberrant collagen secretion (Boyadjiev et al., 2006). These studies suggest that secretion of collagen or large cargo, though using the same basic transport machinery as other cargoes, could be especially sensitive to impairments in that machinery.

The fruit fly *Drosophila*, in which Tango1 was first found, provides a very distinct advantage for studying the early secretory pathway in the form of limited gene redundancy compared with mammals (Kondylis and Rabouille, 2009). For instance, single *Sar1* and *Sec23* homologues are found in *Drosophila*. Similarly, only one Tango1 protein exists in *Drosophila*, in contrast to the presence of multiple TANGO1-like proteins with possible overlapping functions in humans. In addition, most proteins shown to play an essential role in secretory pathway function and organization have homologues encoded in the *Drosophila* genome as well, including Rab small GTPases, COPI and COPII coat components, SNAREs, Golgi matrix proteins, and Golgins. One of the main differences in secretory pathway organization between mammalian and *Drosophila* cells is that in mammals, ERES-derived vesicles fuse to form an ERGIC, where cargo transits en route to a single juxtanuclear Golgi ribbon. In flies, however, Golgi elements remain dispersed throughout the cytoplasm in close proximity to ERESs, forming ERES–Golgi units (Ripoche et al., 1994; Kondylis and Rabouille, 2009). Because this mode of organization is characteristic not just of flies, but probably of all nonmammalian animals and also plants (Brandizzi and Barlowe, 2013), it is certain that ERES–ERGIC–Golgi secretory pathway organization in mammals is an elaboration on an ancestral, more simple theme represented by functionally independent ERES–Golgi units (Glick and Nakano, 2009).

Besides its advantages for secretory pathway studies, the fruit fly *Drosophila* has strongly emerged in recent years as a convenient model to study the biology of collagen and the extracellular matrix. Compared with the 28 types of collagen found in mammals, *Drosophila* possesses a reduced complement of collagens, consisting of basement membrane Collagen IV and Multiplexin (Hynes and Zhao, 2000). Expression of Multiplexin, related to Collagens XV and XVIII, is restricted to the heart and central nervous system and is dispensable for viability (Meyer and Moussian, 2009). Collagen IV, in contrast, is abundantly present in all fly tissues. In *Drosophila*, as in all animals, Collagen IV is the main component of basement membranes, polymers of extracellular matrix proteins that underlie epithelia and surround organs and provide structural support to tissues (Yurchenco, 2011; Kelley et al., 2014). *Drosophila* Collagen IV is a heterotrimer composed of α chains encoded by *Collagen at 25C* (Cg25C; α1 chain) and *viking* (Vkg; α2 chain; Natzle et al., 1982; Fessler and Fessler, 1989). The length of the *Drosophila* Collagen IV trimer is 450 nm, with a predicted molecular mass of 542.4 kD and increased flexibility caused by imperfections of the triple helix (Lunstrum et al., 1988).

Having shown previously that *Drosophila* Tango1 is required for secretion of Collagen IV by fat body cells, their main source in the *Drosophila* larva (Pastor-Pareja and Xu, 2011), we set out to characterize the expression of Tango1, loss-of-function phenotype, and specificity toward Collagen IV. In the course of our study, we found that Tango1 is required to maintain the size and integrity of ERES–Golgi units, its loss of function impairing not only Collagen IV secretion, but also general secretion.

Results

Spatial organization of cargo transport in the center of *Drosophila* ERESs

To better understand the function of Tango1 in *Drosophila* secretion, we decided to first analyze the localization of Tango1 at ERESs and its relation with other proteins in ERES–Golgi units. In conventional light microscopy (for instance, Fig. S1) Tango1-positive structures appear as puncta in which it is possible to distinguish a concave or toroidal shape. To increase resolution in our analysis, we used super-resolution structured illumination microscopy (SIM). When imaged through SIM, ERESs in fat body cells marked by Tango1 appear as regularly sized, ring-shaped, somewhat reticular but continuous structures of ∼1 µm in diameter lying in close proximity or direct contact with one or two smaller distinct structures labeled by cis-Golgi marker GM130 (Fig. 1 A). Analysis of ERES protein Sec16, present in rings at the base of budding COPII carriers (Bharucha et al., 2013), confirmed localization of Tango1 at ERES (Fig. 1 B). Importantly, COPII component Sec23, mediating assembly of ER-to-Golgi carriers, localized to a central region of the ERES cup encircled by Tango1 in 95.2% of ERES (Fig. 1 C; $n = 374$). Simultaneous imaging of cis-Golgi marker Gmap and Sec23 allowed us to visualize the cis-Golgi and COPII-positive structures as distinct objects at the center of the Tango1 ring (Fig. 1 D). Finally, Rab1, a Rab-GTPase involved in ER-to-Golgi transport (Tisdale et al., 1992), concentrated toward the center of the Tango1 ring overlapping cis-Golgi (Fig. 1 E), further supporting that transfer of cargo occurs at the center of ERES cups. In summary, our analysis of Tango1 and other markers confines the transfer of cargo from ER to Golgi to a narrow region in the center of Tango1 rings (Fig. 1 F). Furthermore, when the size of Collagen IV and other large cargoes is taken into account, our analysis strongly suggests that structures identified by Sec23 correspond to single large carriers or tubular connections between the ERES and Golgi.

Requirement of *Drosophila* Tango1 in general secretion

To functionally investigate the function of Tango1 at ERES we knocked down its expression in the fat body, the tissue

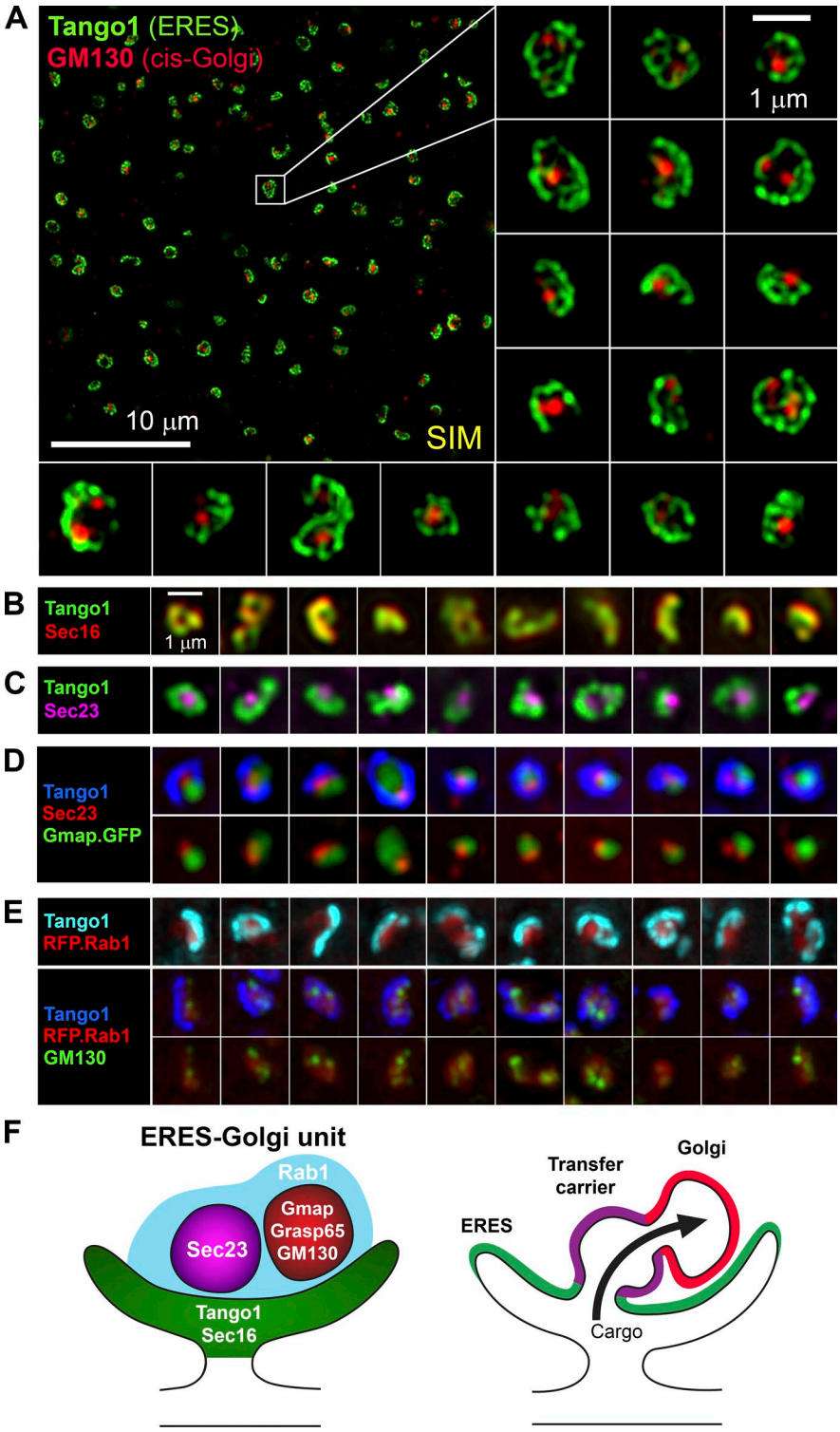

Figure 1. **Imaging of ERES–Golgi units through SIM microscopy.** (A) Image of L3 fat body stained with anti-Tango1 and anti-GM130 antibodies obtained through super-resolution SIM imaging. Examples of individual ERES–Golgi units are shown at higher magnification. Images are maximum intensity projections of two to five confocal sections. (B) ERESs visualized through staining with anti-Sec16 (ERES marker) and anti-Tango1. (C) ERES visualized through staining with anti-Sec23 (COPII coat) and anti-Tango1. (D) ERES–Golgi units visualized with anti-Tango1, anti-Sec23, and Gmap.GFP (GFP-trap insertion into *Gmap* gene). (E) Localization of Rab1 (*Cg>RFP.Rab1*) in relation to ERESs (anti-Tango1) and cis-Golgi (anti-GM130). (F) Organization of ERES–Golgi units as deduced from SIM images above (A–E).

producing most Collagen IV in *Drosophila* larvae. Tango1 knockdown (*Tango1*^{i}) efficiently eliminated the expression of Tango1 (Fig. S1), as revealed by tissue staining with a Tango1 antibody (Lerner et al., 2013). As previously shown (Pastor-Pareja and Xu, 2011), *Tango1*^{i} fat body cells intracellularly retain Collagen IV (Fig. 2, A and B), a heterotrimer consisting of the α1 chain Cg25C and the α2 chain Vkg, assessed with a Vkg.GFP protein trap fusion and an anti-Cg25C antibody. To test whether Tango1 was specifically required for secretion of the Collagen IV assembled trimer, we knocked down expression of Prolyl-4-hydroxylase PH4αEFB, which is required for Collagen IV trimerization in the fat body (Pastor-Pareja and Xu, 2011). We found that *Tango1*^{i} fat body cells retained the Vkg chain when trimerization was prevented by PH4αEFB knockdown (Fig. 2 C). This shows that monomeric Collagen IV chains and not just trimers are secreted in a Tango1-dependent manner.

Compelled by the previous result, we set out to further test the specificity of the requirement of Tango1 in secretion

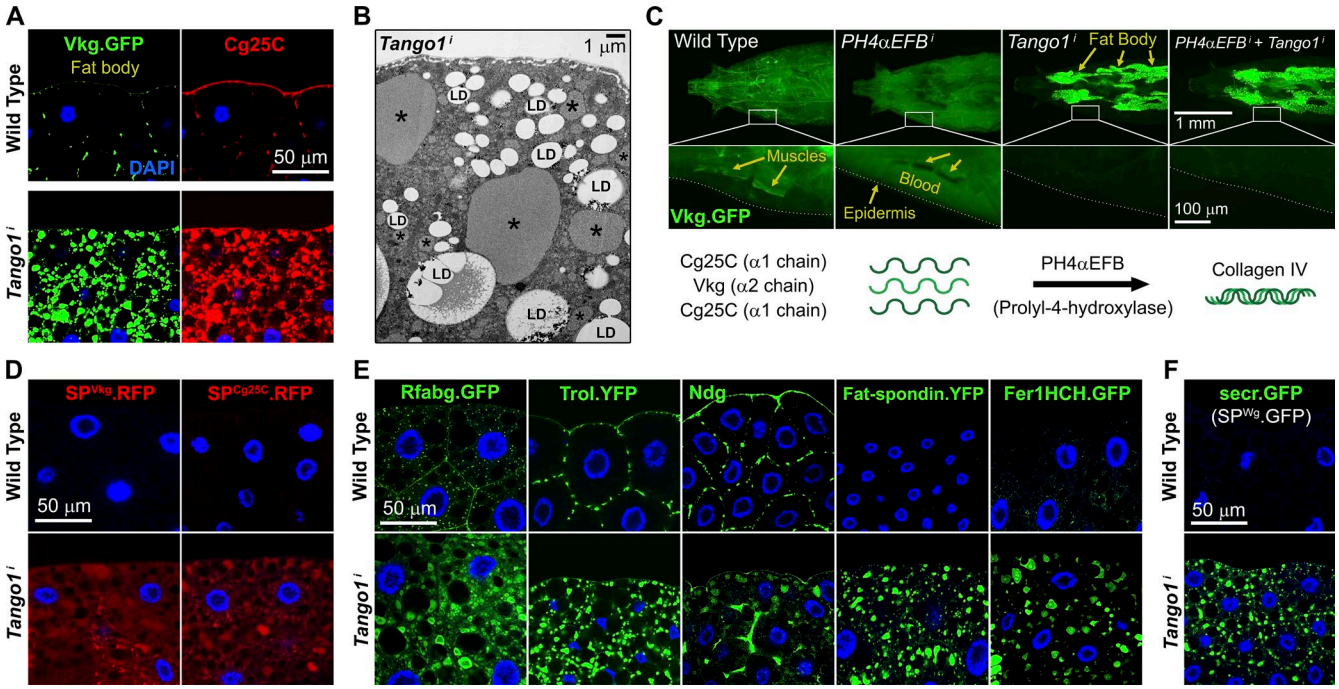

Figure 2. **Tango1 knockdown impairs general secretion in fat body cells.** (A) Confocal images of fat body cells from wild-type (top) and *Tango1* knockdown (*BM-40-SPARC-GAL4 > UAS-Tango1^{i}*, bottom) third-instar larvae (L3 stage) showing distribution of Collagen IV chains α2 (Vkg.GFP, left) and α1 (anti-Cg25C, right). Nuclei were stained with DAPI. (B) Electron micrograph of *Cg>Tango1^{i}* fat body. Asterisks mark cargo-filled dilated ER. LD, lipid droplets. (C) Distribution of Collagen IV (Vkg.GFP) in wild-type, *BM-40-SPARC>PH4αEFB^{i}*, *>Tango1^{i}*, and double *>PH4αEFB^{i}+Tango1^{i}* larvae. Insets magnified in the bottom panels show Vkg.GFP localization to muscle basement membranes (wild type) or diffuse blood signal (*PH4αEFB^{i}*). (D) Wild-type (top) and *Tango1^{i}* (bottom) fat body cells expressing RFP coupled to signal peptides of Vkg (*Cg>SP^{Vkg}.RFP,* left) and Cg25C (*Cg>SP^{Cg25C}.RFP*, right). (E) Wild-type and *Tango1^{i}* fat body cells showing distribution of Rfabg (Apo-B, *Rfabg.sGFP$^{fTRG.900}$*), YFP-tagged Trol (Perlecan, *trol$^{CPTI-002049}$.YFP*), Nidogen (anti-Ndg staining), Fat-spondin (*fat-spondin^{CPTI001685}.YFP*), and Ferritin (*Fer1HCH^{G188}.GFP*). (F) Wild-type and *Tango1^{i}* fat body cells expressing secr.GFP (*BM-40-SPARC>secr.GFP*, signal peptide of Wingless coupled to GFP).

and found that all secretory cargoes we tested were defectively secreted by *Tango1^{i}* cells (see Table S1 for molecular weights of cargoes). Tested cargoes were RFP coupled to Vkg or Cg25C signal peptides (Fig. 2 D), ApoB-related Rfabg, the basement membrane components Perlecan (Trol) and Nidogen (Ndg), Fat-spondin, Ferritin (Fer1HCH; Fig. 2 E), and the widely used *Drosophila* secretion marker secr.GFP, consisting of GFP coupled to the signal peptide of Wingless (Fig. 2 F). To test whether the general secretion defect was secondary to Collagen IV retention or ER protein overloading, we overexpressed Collagen IV α1 monomer Cg25C or the LanB1 γ subunit or the Laminin trimer, which caused intracellular accumulation of the overexpressed proteins but failed to detect retention of secr.GFP in the same cells (Fig. S2). These results indicate that Tango1 has a role in general secretion by fat body cells.

To further explore the role of Tango1 in secretion, we stained larval tissues with anti-Tango1 antibody and found that, in contrast to the restricted expression of Collagen IV (Pastor-Pareja and Xu, 2011), Tango1 was expressed in all tissues examined (Fig. 3 A). The highest levels of Tango1 expression were found in the salivary gland, an organ devoted to the fast, abundant secretion of glue proteins at the onset of metamorphosis. *Tango1^{i}* salivary glands were indeed unable to secrete Sgs3 glue protein to the gland lumen (Fig. 3 B). In the wing imaginal disc, the larval precursor of the adult wing epidermis, secretion of the extracellular signaling protein Hedgehog (Fig. 3 C) and the secretion marker secr.GFP (Fig. 3 D) were defective in *Tango1^{i}* cells as well. From all of the aforementioned results, we conclude that Tango1 in *Drosophila* is widely expressed, its loss impairing not only the secretion of collagen, extracellular matrix, or large proteins, but also general secretion.

Tango1 loss differentially affects secretion of Collagen IV

Our observation of general secretion defects by *Tango1^{i}* cells in *Drosophila* contrasts with the limited secretion defects seen in the absence of members of the MIA/cTAGE family in mammals. To explore this issue, we compared the effects of Tango1 on secretion of Collagen IV and other proteins. For this purpose, we quantified Collagen IV retention in *Tango1^{i}* fat body cells and compared the retention of secreted RFP (SP^{Vkg}.RFP) expressed in the same cells. In this way, we found that *Tango1^{i}* cells retained Collagen IV (Vkg.GFP) to a larger extent than secreted RFP, as indicated by the increased Collagen IV–to-RFP signal ratio in *Tango1^{i}* cells when compared with that same ratio in *Sec23^{i}* or *Sar1^{i}* cells (Fig. 4 A). This result indicates that the requirement of Tango1 in RFP secretion compared with Collagen IV is less stringent. To confirm this differential effect of Tango1 on Collagen IV secretion in a second cell type, we additionally compared the effects on secretion of Collagen IV, secreted GFP, and the transmembrane secretion marker VSVG in *Tango1^{i}* blood cells. Confirming the results in fat body cells, *Tango1^{i}* blood cells showed retention of Collagen IV similar to *Sec23^{i}* or *Sar1^{i}* blood cells but milder retention of secreted GFP and VSVG than *Sec23^{i}* or *Sar1^{i}* blood cells (Fig. 4 B).

Our results so far showed that although Tango1 is present in all cell types and involved in general secretion, but also

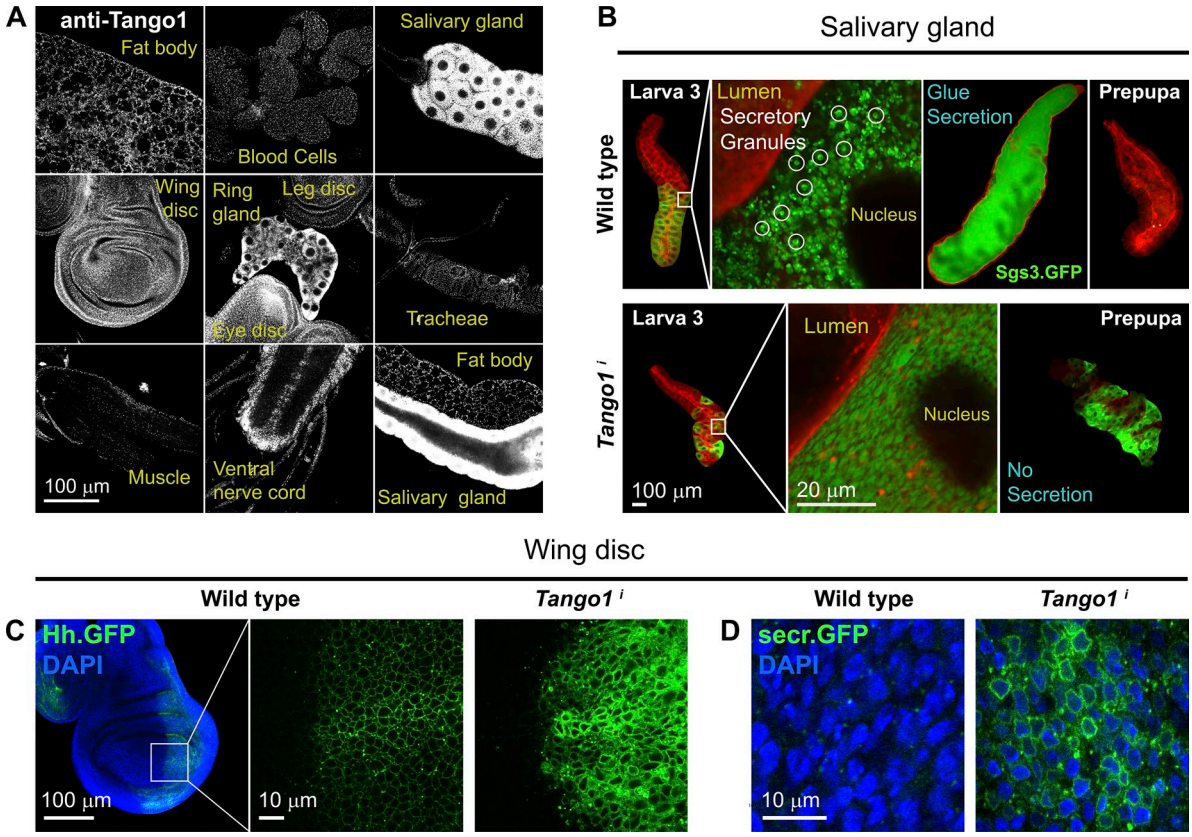

Figure 3. **Tango1 is widely expressed and required for secretion in salivary glands and disc cells.** (A) Expression of Tango1 in different tissues of the L3 larva (anti-Tango1 staining). (B) Localization of glue protein Sgs3 (Sgs3.GFP) in late L3 and pre-pupal salivary glands of wild-type and *He>Tango1*^{i} animals. No individualized secretory granules are seen in *Tango1*^{i} glands, and Sgs3.GFP remains inside cells after the onset of metamorphosis. The membrane marker myr.RFP is shown in red. (C) Confocal images of control and *Tango1*^{i} wing discs expressing Hedgehog.GFP in their posterior compartment (*hh>hh.GFP*). (D) Confocal images of wild-type and *Tango1*^{i} wing disc cells expressing secr.GFP (*rn>secr.GFP*).

that this involvement may not be an absolute requirement for secretion of all possible cargoes. Consistent with this, *Sec23* and *Sar1* mutants show strong defects in the embryonic epidermis and die before becoming larvae (Abrams and Andrew, 2005; Tsarouhas et al., 2007; Kumichel et al., 2015), whereas mutants for *Tango1*^{GS15095}, an allele caused by a transposon insertion in the first exon of *Tango1* (Fig. S3 A), die in the larva 1 stage (Tiwari et al., 2015; confirmed by us). Additionally, genetic mosaic experiments in the eye disc showed that *Sar1* mutant clones could not be recovered, indicating strict cell lethality, whereas *Tango1*^{GS15095} mutant clones could be examined despite reduced viability (Fig. S3 B). Finally, in another mosaic experiment, we observed that *Tango1*^{GS15095} blood cells were capable of releasing secreted RFP to the blood (Fig. S3 C). All of the aforementioned data support that some cargoes like Collagen IV may show higher dependence on Tango1 for their secretion.

Tango1 loss causes smaller ERESs uncoupled from Golgi

Having characterized ERES–Golgi unit organization in the wild type, we examined *Tango1*^{i} fat body cells to ascertain the effect of Tango1 loss on ERES–Golgi units. *Tango1*^{i} cells showed a striking decrease in the size of ERESs, marked by Sec16.GFP, apparent in both conventional confocal light microscopy (Fig. 5 A) and SIM (Fig. 5 B). In addition, ERESs and cis-Golgi, marked by GM130, appeared frequently separate from each other in contrast to the tight apposition found in the wild type. The same phenotypes of ERES size decrease and ERES–Golgi unit dissociation were observed in *Tango1*^{GS15095} homozygous mutants (Fig. 5 C), confirming the involvement of Tango1 in maintaining ERES size and ERES–Golgi unit integrity. Quantification of ERES–Golgi unit dissociation in *Tango1*^{i} fat body cells showed that less than half of ERESs, marked by Sec16, were found in proximity to cis-Golgi markers or Rab1, whereas normal association of Rab1 with cis-Golgi was not affected (Fig. 5, D and E). These results reveal a requirement of Tango1 in the maintenance of ERES–Golgi units.

Cytoplasmic Tango1 directs ERES localization and can rescue Tango1 knockdown

To further characterize the function of Tango1 in ERES–Golgi unit organization, we analyzed the requirements of its domains for proper localization to ERESs. To do this, we expressed in *Drosophila* S2 cells several constructs in which different parts of the protein were fused to GFP (Fig. 6, A and B). As previously shown for mammalian TANGO1 (Saito et al., 2009), deletion of the cytoplasmic domain of Tango1 (Tango1$^{\Delta CYT}$) abolished ERES localization. Interestingly, the cytoplasmic part of Tango1 (Tango1^{CYT}), lacking the signal peptide, the intraluminal part and transmembrane domains of the protein, was able to localize to ERESs, showing that the cytoplasmic region of Tango1 is both necessary and sufficient to ensure proper

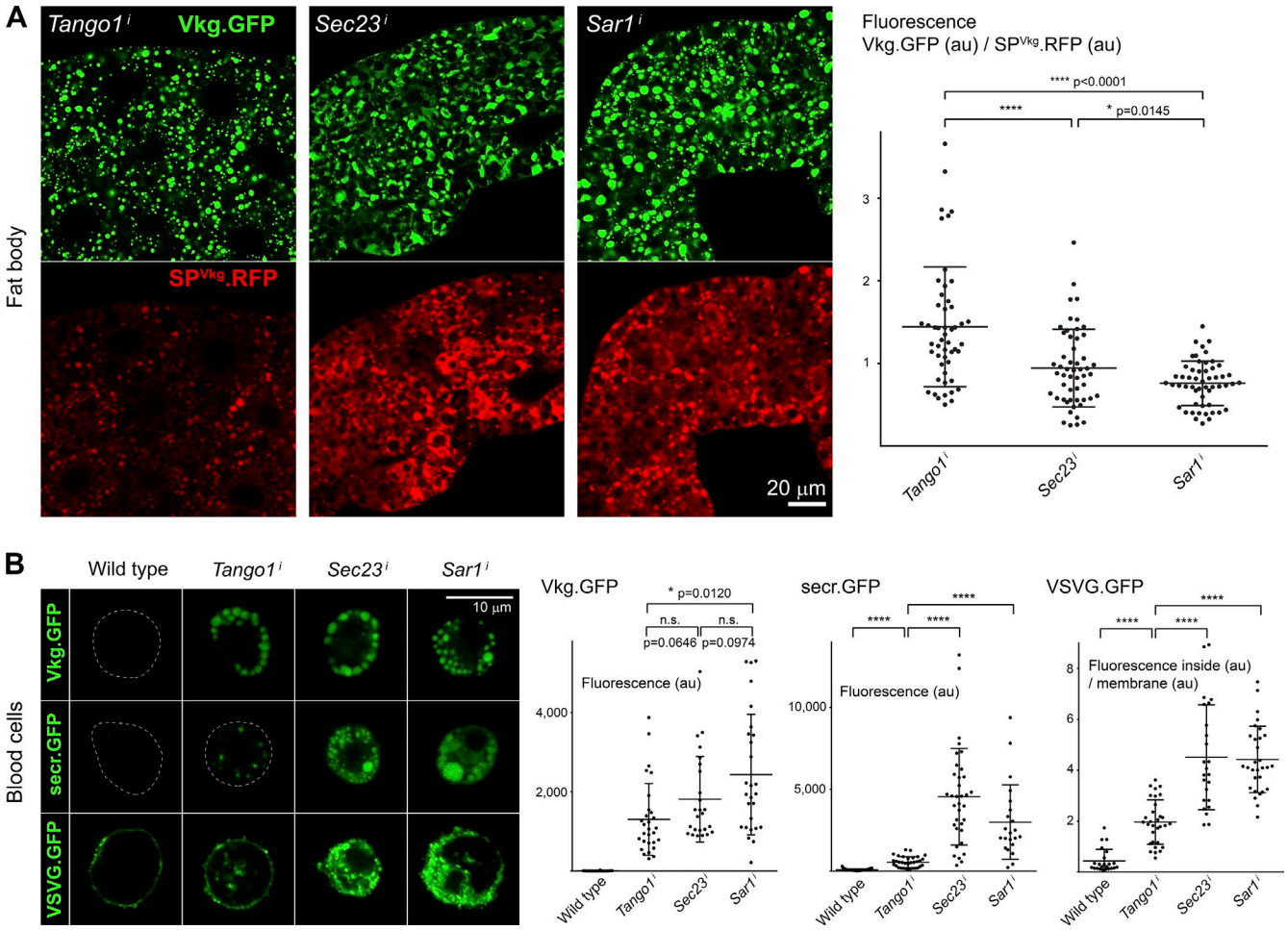

Figure 4. **Tango1 differentially affects the secretion of Collagen IV.** (A) Confocal images of fat body cells from *BM-40-SPARC>Tango1*^{i}, *>Sec23*^{i}, and *>Sar1*^{i} larvae showing distribution of Collagen IV.GFP (Vkg.GFP) and RFP (signal peptide of Vkg coupled to RFP). Graphs show quantification of fluorescent signal ratio, each dot representing an individual cell ($n > 50$). Horizontal lines and error bars represent mean and standard deviation, respectively. P-values correspond to two-tailed *t* tests. au, arbitrary units. (B) Confocal images of hemocytes (blood cells) from wild-type, *BM-40-SPARC>Tango1*^{i}, *>Sec23*^{i}, and *>Sar1*^{i} larvae showing distribution of Vkg.GFP (top), secr.GFP (middle), and VSVG.GFP (bottom). Graphs show quantification of fluorescent signal as above (A; $n \geq 22$). au, arbitrary units.

localization of the protein. Further dissection of the localization properties of the cytoplasmic domain of Tango1 revealed that the coiled-coil region of the protein could localize to ERESs by itself, whereas the most C-terminal region containing the proline rich domain could not (Fig. 6, A and B).

To functionally test the role of the cytoplasmic domain of Tango1 in ERES–Golgi unit organization in vivo, we constructed transgenic flies expressing GFP-tagged Tango1^{CYT} in the larval fat body. Confirming in vivo the result previously obtained in S2 cells, Tango1^{CYT} correctly localized to ERESs (Fig. 6 C). In addition, expression of this Tango1^{CYT} construct was able to rescue lethality and defective Collagen IV secretion caused by knockdown of Tango1 with a double-stranded RNA that targeted endogenous Tango1, but not GFP.Tango1^{CYT} (Fig. 6 D and Table S2). This latter result strongly supports a function of the cytoplasmic domain of Tango1 in organizing ERES–Golgi units and facilitating secretion in a way that does not necessarily require the transmembrane and ER intraluminal domains of the protein, through which Tango1 is supposed to bind cargo.

Tango1 overexpression increases ERES size and number

Trying to assess the role of Tango1 in ERES morphogenesis, we decided to study the effects of increased Tango1 expression. Overexpression of Tango1 in a medial stripe of cells of the wing disc under control of *ptc-GAL4* caused an increase in both the density and size of ERESs compared with more lateral cells expressing a normal dose of Tango1 (Fig. 7 A). Overexpression in the fat body of GFP-tagged Tango1 and Tango1^{CYT} gave rise to strikingly enlarged ERESs and increase in their mean size (Fig. 7, B–D). Finally, in blood cells, where comparison of individual cells is most convenient, the overexpression of Tango1 caused a large increase in the amount of Golgi units, as shown by staining with cis-Golgi marker anti-Gmap (Fig. 7 E). Altogether, these results show that Tango1 is a potent promoter of ERES morphogenesis that can influence ERES size and number of ERES–Golgi units. Our data also suggest that varying levels of Tango1 expression may be responsible for differences in ERES size and number among cell types.

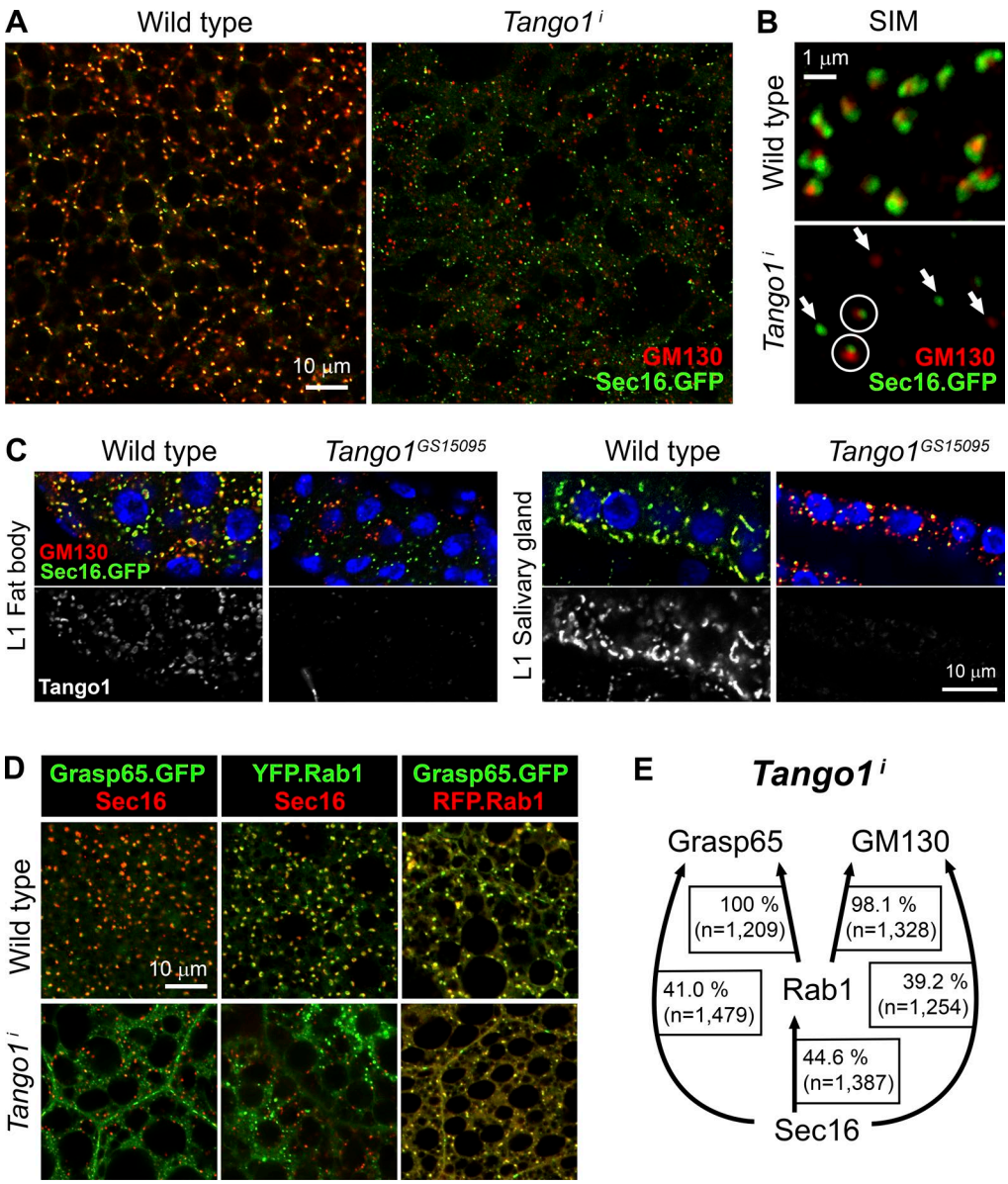

Figure 5. **Loss of Tango1 produces smaller ERESs uncoupled from Golgi.** (A) Confocal images of wild-type and *Cg>Tango1*^{i} fat body cells stained with anti-GM130 and expressing Sec16.GFP (transgenic insertion of BAC construct containing *Sec16* locus modified by the addition of C-terminal GFP). (B) SIM images of wild-type and *Cg>Tango1*^{i} fat body showing localization of Sec16.GFP and GM130. Arrows mark separate Sec16- and GM130-positive structures. The two structures where Sec16- and GM130-positive structures maintain proximity are marked by circles. (C) Confocal images of fat body (left) and salivary gland (right) cells from wild-type and mutant *Tango1*^{GS15095} first instar (L1) larvae showing localization of Sec16.GFP and GM130. Tissues were stained with anti-Tango1 antibody. Nuclei are in blue (DAPI). (D) Confocal images of fat body from wild-type (top) and *Cg>Tango1*^{i} (bottom) larvae showing localization of the cis-Golgi marker Grasp65 (*Cg>Grasp65.GFP*), the ERES marker Sec16, and the GTPase Rab1 (*Cg>YFP.Rab1* and *Cg>RFP.Rab1*). (E) Quantification of defects in ERES–Golgi unit organization in *Cg>Tango1*^{i} fat body cells. The percentage of Sec16 puncta that are found next to Rab1, Grasp65, and GM130 puncta is indicated. Idem for Rab1-positive puncta next to Grasp65 and GM130 puncta.

Multiple interactions of Tango1 at the ERES–Golgi interface

Given that Tango1 loss affected ERES size and ERES–Golgi unit integrity, we finally decided to investigate possible interactions of Tango1 that could impact ERES–Golgi unit organization. It has been shown in mammalian cells that Tango1 interacts with cTAGE5 (Saito et al., 2011), like Tango1, a member of the MIA/cTAGE family. Because *Drosophila* Tango1 is the only member of the MIA/cTAGE family member present in this organism, we hypothesized that Tango1 might be capable of self-interacting. To test this, we coexpressed in the larval fat body C-terminally HA-tagged and FLAG-tagged versions of Tango1 and found that they coimmunoprecipitated (Fig. 8 A). The cytoplasmic domain of Tango1 contains a coiled-coil region, like Golgins. Golgins have been shown to form a matrix up to 300 nm away from Golgi membranes to which incoming vesicles are docked (Gillingham and Munro, 2016). Because of the localization of Rab1 between ERES and cis-Golgi and its uncoupling from ERES in *Tango1*^{i} cells, we also tested a possible interaction of Tango1 with Rab1, similar to the way GM130 and other Golgins interact with Rab-GTPases. Indeed, we were able to coimmunoprecipitate Rab1 and Tango1 from fat body extracts (Fig. 8, B and C; see Fig. S4 for Rab1 antibody validation). Tango1 additionally coimmunoprecipitated with cis-Golgi proteins Grasp65

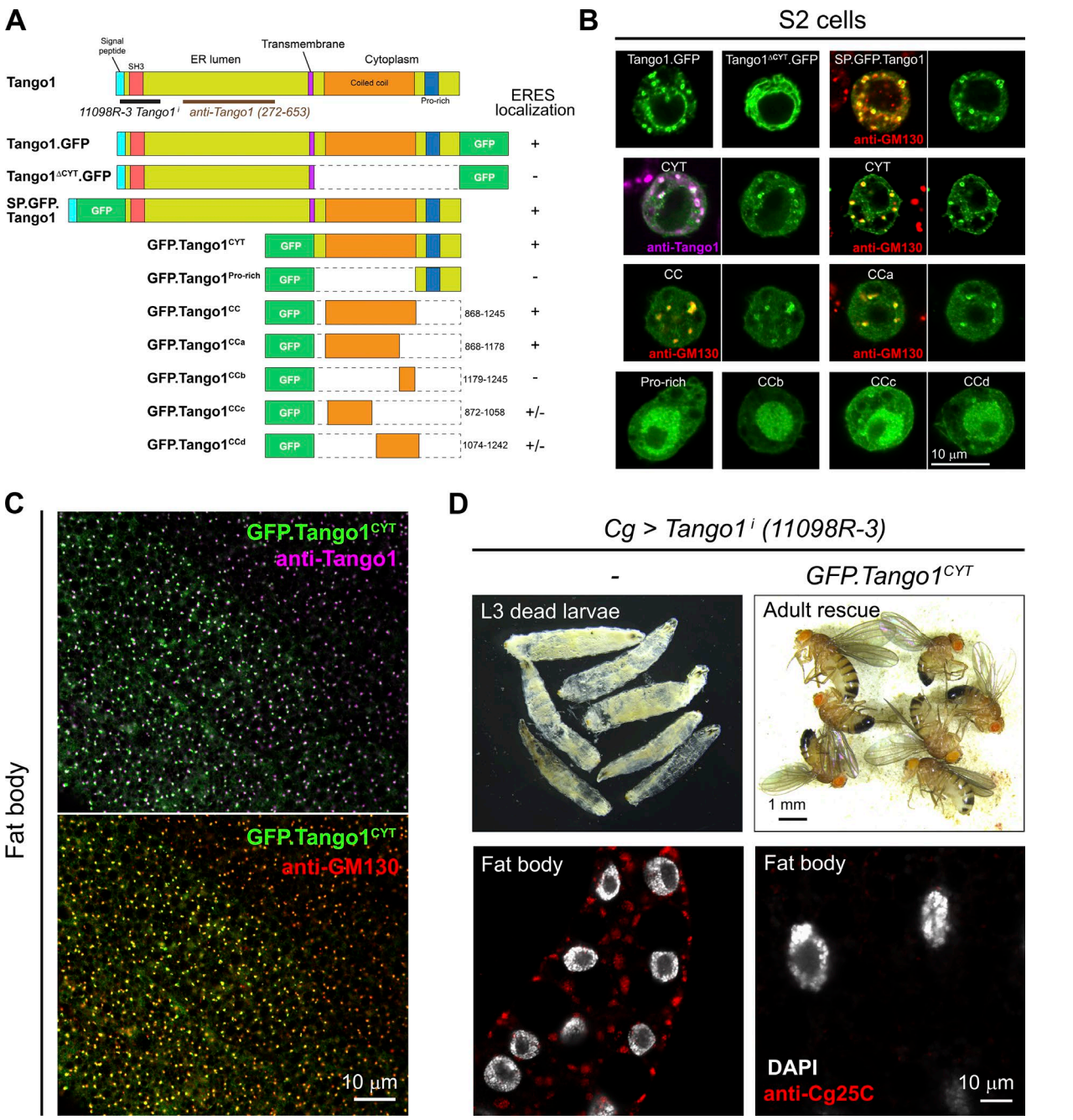

Figure 6. **The cytoplasmic part of Tango1 directs ERES localization and can rescue Tango1 loss.** (A) Graphic representation of GFP-tagged Tango1 constructs generated in this study. The ability to localize to ERESs is indicated on the right. (B) Confocal images of *Drosophila* S2 cells transfected with the indicated constructs. GM130 and Tango1 antibody staining used to confirm ERES–Golgi localization. (C) Localization of Tango1^{CYT} (*Cg>GFP.Tango1*^{CYT}) in fat body cells stained with anti-Tango1 and anti-GM130. Note that Tango1 antibody was raised against a part of Tango1 not present in Tango1^{CYT}. (D) Rescue of *Tango1*^{i} larval lethality and Collagen IV retention by GFP.Tango1^{CYT}. See also Table S2. Note that the double-stranded RNA used here targets a part of the Tango1 sequence not present in Tango1^{CYT}.

(Fig. 8 D) and GM130 (Fig. 8 E), the latter known to bind Rab1 and Grasp65 (Fig. 8, F and G). Finally, similar to mammalian TANGO1 (Saito et al., 2009), we confirmed the interaction of Tango1 with the COPII coat machinery, as Tango1 coimmunoprecipitated with Sar1 (Fig. 8 H). In all, our coimmunoprecipitation data confirm the close interrelations among ERES, COPII carriers, and Golgi while lending support to a model (Fig. 8 I) in which Tango1, through multiple interactions of its cytoplasmic domain, spatially coordinates these three compartments, thus enhancing the transit of cargo among them.

Discussion

In this study, we investigated the expression, localization, and role in secretion of Tango1, the only member of the MIA/cTAGE family in *Drosophila*. Our imaging of ERESs through super-resolution microscopy revealed close proximity of COPII carriers and cis-Golgi elements in the center of Tango1 rings (see also companion paper by Raote et al., 2017, in this issue). When we examined the effects of Tango1 loss, we found that ERESs were reduced in size and frequently uncoupled from

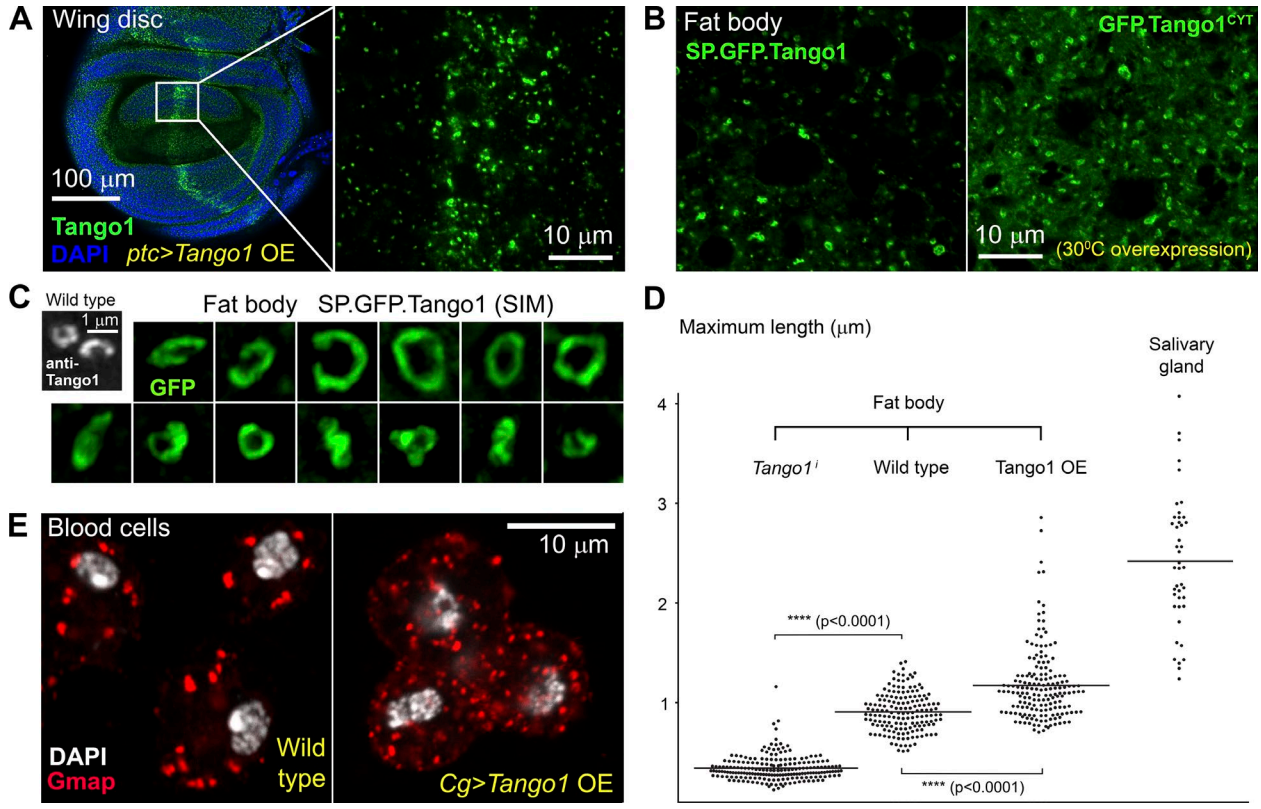

Figure 7. **Tango1 overexpression increases ERES size and number.** (A) Confocal images of a wing disc overexpressing (OE) Tango1 in a medial stripe of cells (*ptc>Tango1*) and stained with anti-Tango1. Area inside the square is shown at higher magnification on the right. (B) Confocal images of fat body expressing Tango1 GFP-tagged at the N terminus after its signal peptide (*Cg>SP.GFP.Tango1*, left) and the cytoplasmic portion of Tango1 GFP-tagged at the N terminus (*GFP.Tango1*^{CYT}, right). (C) Examples of enlarged ERESs caused by expression of SP.GFP.Tango1 imaged through SIM. Two normal-sized wild-type ERESs are shown for comparison. (D) Quantification of individual ERES size in *Cg>Tango1*^{i} fat body (n = 202), wild-type fat body (n = 163), Tango1-overexpressing fat body (Cg>SP.GFP.Tango1; n = 174), and wild-type salivary glands (n = 43). Horizontal lines indicate mean size. Images were analyzed with ImageJ, and apparent maximum lengths of the structures were manually measured with the line tool. P-values from two-tailed t tests are shown. (E) Confocal images of blood cells from wild-type (left) and *Cg>SP.GFP.Tango1* larvae (right) stained with anti-Gmap (cis-Golgi marker).

Golgi, indicating a requirement of Tango1 in the normal organization of ERES–Golgi units. Moreover, supporting an important role of Tango1 in the morphogenesis of *Drosophila* ERESs, overexpression of Tango1 created more and larger ERESs.

Overall, our results are consistent with a model in which the spatial organization of the ERES–Golgi interface provided by Tango1's multiple interactions helps build enlarged COPII carriers that canalize traffic in the center of ERESs. The proximity of ERESs and Golgi in *Drosophila* leads us to additionally propose that direct ERES–Golgi contact might be the way in which large cargo normally transfers from the ER to the Golgi in flies. Direct contact between ER and Golgi has been suggested as a mode of ER-to-Golgi transport in the yeast *Saccharomyces cerevisiae* (Kurokawa et al., 2014) and in plants (daSilva et al., 2004), where ERESs and Golgi are, like in *Drosophila*, closely juxtaposed and possibly attached physically through a matrix (Sparkes et al., 2009; Brandizzi and Barlowe, 2013). ERES–ERGIC contact also has been suggested as a transport mechanism in mammals (Malhotra and Erlmann, 2015). Careful electron tomography analysis and in vivo imaging could be used in the future to investigate in more detail the dynamics of cargo transfer among ERESs, COPII carriers, and Golgi at the center of Tango1 rings. Given the necessity to secrete not only Collagen IV or lipoprotein particles but also giant cuticular proteins like the 2,500-mol-wt protein Dumpy (Wilkin et al., 2000), ER-to-Golgi carriers in *Drosophila* must be necessarily large. Taking into account this and the narrow space in which *Drosophila* ERES–Golgi transport takes place, we consider it possible that such large carriers start fusion with the Golgi before having separated from the ERES, effectively creating intermittent tubular connections.

Our experiments, importantly, revealed a wider role in secretion for Tango1, its knockdown causing intracellular retention of the multiple cargoes we examined. Thus, large carriers or tubular connections built with the assistance of Tango1 may mediate not only the transport of large cargo, but also a significant portion of the total flow of general cargo. This is in contrast to the specific roles in secretion of collagens (TANGO1, TANGO1S, and cTAGE5) or lipoprotein particles (TANGO1 and TALI) proposed for mammalian members of the MIA/cTAGE family. Apart from Collagen IV (Pastor-Pareja and Xu, 2011), the ECM proteins Perlecan (Lerner et al., 2013), Tiggrin (Zhang et al., 2014), SPARC (Tiwari et al., 2015), and Laminin (Petley-Ragan et al., 2016) were previously observed to accumulate intracellularly in the absence of *Drosophila* Tango1, raising the possibility that these defects were secondary to Collagen IV retention or, alternatively, that Tango1 were required for secretion of large ECM proteins in general. Our results, however, show that small non-ECM cargoes like plain GFP were inefficiently secreted in the absence of Tango1 as well. Further supporting a general role of *Drosophila* Tango1 in secretion, Tango1 is expressed in all tissues of the larva, inconsistent

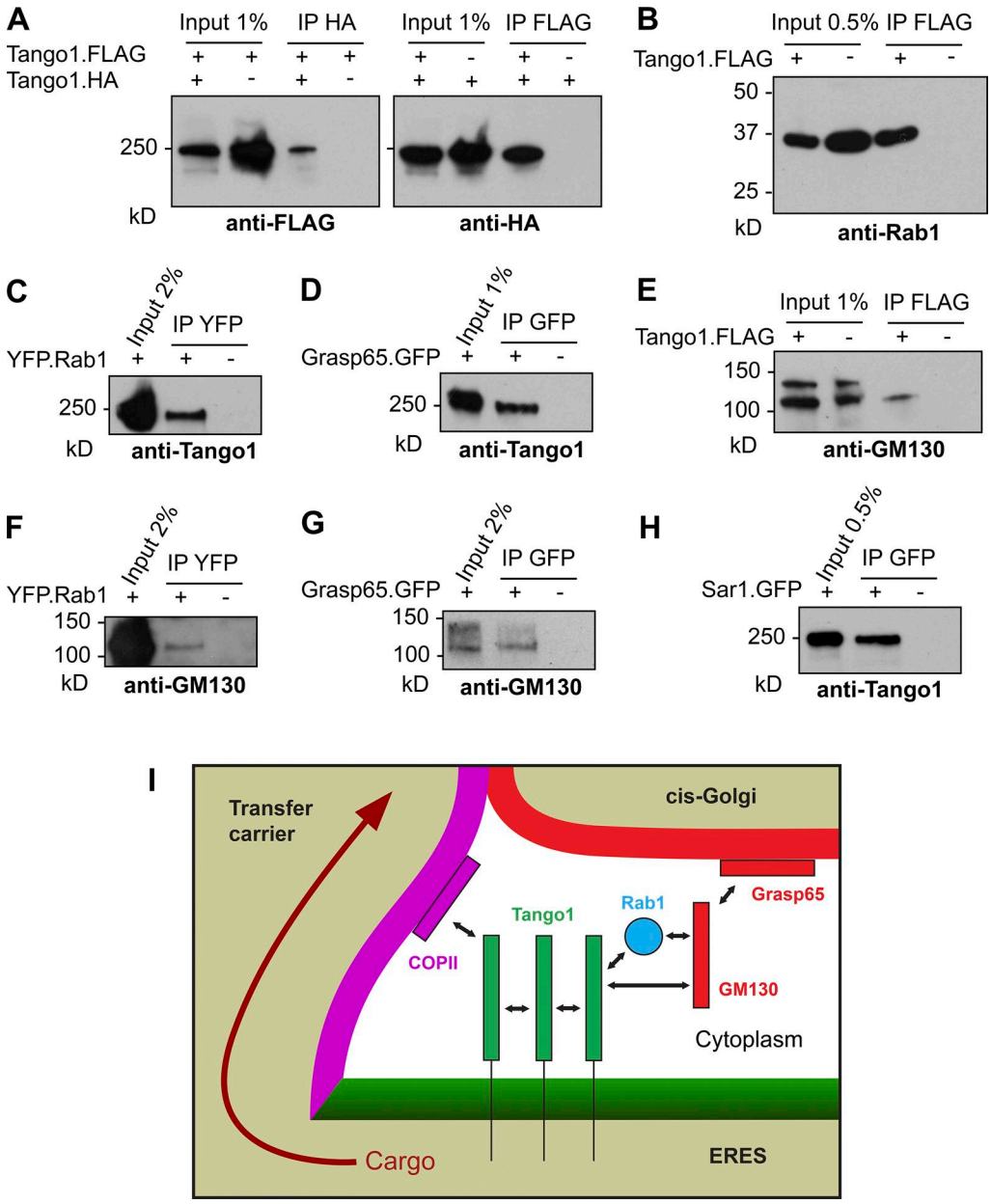

Figure 8. **Multiple interactions of Tango1 at the ERES–Golgi interface.** (A) Tango1.HA (left) and Tango1.FLAG (right) were immunoprecipitated from L3 fat body lysates. Immunoprecipitates (IP) were Western blotted with anti-FLAG (left) and anti-HA (right) antibodies. (B) Tango1.FLAG fat body immunoprecipitates, Western blotted with anti-Rab1 (see Fig. S4 for antibody validation). (C) YFP.Rab1 fat body immunoprecipitates, Western blotted with anti-Tango1. (D) Grasp65.GFP fat body immunoprecipitates, Western blotted with anti-Tango1. (E) Tango1.FLAG fat body immunoprecipitates, Western blotted with anti-GM130. (F) YFP.Rab1 fat body immunoprecipitates, Western blotted with anti-GM130. (G) Grasp65.GFP fat body immunoprecipitates, Western blotted with anti-GM130. (H) Sar1.GFP fat body immunoprecipitates, Western blotted with anti-Tango1. (I) Static model depicting Tango1 interactions (with itself, COPII, Rab1, and cis-Golgi peripheral proteins GM130-Grasp65) and possible role of Tango1 in maintaining Golgi proximity and ERES–Golgi organization for increased secretory capacity.

with a relation with specific cargoes. The highest expression of Tango1 was found in the salivary gland, a dedicated secretory organ where genes encoding secretory pathway components are highly expressed as a group, including COPII and COPI genes (Abrams and Andrew, 2005). It would seem, therefore, that Tango1 expression correlates with secretory activity, but not with Collagen IV secretion because Collagen IV is not expressed in the salivary gland (Pastor-Pareja and Xu, 2011).

Supporting both an organizing function of Tango1 at the ERES–Golgi interface and a wider role in secretion, the cytoplasmic part of Tango1 could rescue Tango1 loss in the fat body. The result of this rescue experiment additionally posits the question of what is the role of the intraluminal part of the *Drosophila* protein, through which mammalian TANGO1 is thought to interact with cargo. The intraluminal SH3-like domain of Tango1 is conserved among *Drosophila* and mammals, a sure sign of a biological role, and it is possible that this domain in *Drosophila* still has a role in binding cargoes, either directly or through several adaptors. Nonetheless, our results clearly show that Tango1 loss impairs general secretion and that the cytoplasmic part of the protein is by itself capable of enhancing Collagen IV secretion independent of the intraluminal part. Although it is

conceivable that *Drosophila* Tango1 and mammalian TANGO1 have diverged in their function, the possibility that MIA/cTAGE5 family members are partially redundant in facilitating general secretion beyond any roles they may have as specific cargo adaptors is worth considering in light of our findings.

Recently, suppression of mammalian TFG expression has been shown to result in smaller ERESs that remain functional for the export of many secretory cargoes, but not collagen (McCaughey et al., 2016). TFG, a protein first characterized in the roundworm *Caenorhabditis elegans* (Witte et al., 2011), has been proposed to act in mammals by forming oligomeric assemblies that physically join ERESs and ERGIC (Johnson et al., 2015). Human and *C. elegans* TFG have no clear homologue in *Drosophila* (our own BLAST analysis). Conversely, *C. elegans* has no Tango1 homologue (Erives, 2015). This is despite the fact that *C. elegans* possess all four major basement membrane components, numerous collagens, and multiple other large ECM proteins (Kramer, 1994). In this evolutionary context, our work on *Drosophila* Tango1 shows that alternative mechanisms acting in ERES organization may exist in animal cells to increase capacity of ER-to-Golgi transport in terms of both cargo size and the amount of cargo to be secreted. Furthermore, because small COPII vesicles have seldom been observed in animal cells, it is possible that animals have largely abandoned these in favor of larger COPII-dependent carriers built with help from proteins like TFG and Tango1. Such proteins might have initially evolved to enable secretion of metazoan ECM and other large cargoes, creating in the process a mode of transport that increased efficiency of general ER export as well.

Materials and methods

Drosophila strains

Standard fly husbandry techniques and genetic methodologies, including balancers and dominant genetic markers, were used to assess segregation of mutations and transgenes in the progeny of crosses, construct intermediate fly lines and obtain flies of the required genotypes for each experiment (Roote and Prokop, 2013). Cultures were maintained at 25°C in all experiments except the expression of GFP.Tango1^{CYT} (Fig. 8 B), which was maintained at 30°C for increased GAL4-driven expression. The GAL4-UAS binary expression system (Brand and Perrimon, 1993) was used to drive expression of UAS transgenes under temporal and spatial control of transgenic GAL4 drivers *BM-40-SPARC-GAL4*, *Cg-GAL4*, *He-GAL4*, *rn-GAL4*, *hh-GAL4*, and *ptc-GAL4*. Genotypes of animals in all experiments are detailed in Table S3. Stable insertion of transgenic UAS constructs was achieved through standard P-element transposon transgenesis (Rubin and Spradling, 1982) except for *UAS-Tango1.attP2*, which was obtained by att-directed insertion (Groth et al., 2004). *Tango1* mutant eye disc cells and hemocytes were generated through the Flp/FRT and MARCM systems (Xu and Rubin, 1993; Lee and Luo, 2001). The following strains were used: *w^{1118}* (3605; Bloomington *Drosophila* Stock Center); *w Gmap^{KM0132}.GFP* (109702; *Drosophila* Genomics and Genetics Resources); *w ; UAS-RFP.Rab1.3.1* (this study); *y w ; vkg^{G454}.GFP/CyO* (11069; *Drosophila* Genomics and Genetics Resources); *w UAS-myr.RFP* (7118; Bloomington *Drosophila* Stock Center); *w ; BM-40-SPARC-GAL4/TM6B* (gift from H. Bellen, Baylor College of Medicine, Houston, TX); *w ; UAS-Dcr2* (24651; Bloomington *Drosophila* Stock Center); *w ; UAS-myr.RFP* (7119; Bloomington *Drosophila* Stock Center); *w ; UAS-Tango1.RNAi^{VDRC21594}/TM6B*; *w ; UAS-Tango1.RNAi^{NIG11098R}/TM6B*; *w ; UAS-PH4αEFB.RNAi$^{VDRC.v2464}$*; *w ; UAS-PH4αEFB.RNAi$^{VDRC.v2464}$UAS-Tango1.RNAi^{VDRC21594}/TM6B*; *w ; UAS-SP^{Vkg}.RFP.3.1* (this study); *w ; UAS-SP^{Cg25C}.RFP.3.1* (this study); *w ;Cg-GAL4* (7011; Bloomington *Drosophila* Stock Center); *y w ; Rfabg.sGFP$^{fTRG.900}$* (318255; Vienna *Drosophila* Resource Center); *w trol$^{CPTI-002049}$.YFP* (115262; *Drosophila* Genomics and Genetics Resources); *w ; fat-spondin^{CPTI001685}.YFP* (115184; *Drosophila* Genomics and Genetics Resources); *w ; Fer1HCH^{G188}.GFP* (110620; *Drosophila* Genomics and Genetics Resources); *w ; UAS-secr.GFP* (gift from F. Zhang, Nanfang Hospital, Guangzhou, China); *w ; Sgs3.GFP* (5884; Bloomington *Drosophila* Stock Center); *w ; rn-GAL4/TM6B* (7405; Bloomington *Drosophila* Stock Center); *w ; UAS-hh.GFP* and *w ; hh-GAL4* (gifts from I. Guerrero, Centro de Biología Molecular, Madrid, Spain); *w ;UAS-LanB1.RFP.3.1* (this study); *w ;UAS-Cg25C.RFP.3.1* (this study); *w ; UAS-Sec23.RNAi^{VDRC24552GD}*; *w ;UAS-Sar1.RNAi^{VDRC34192G}*; *w ;Ub-VSVG.GFP* (gift from T. Lecuit, Institut de Biologie du Développement, Marseille, France); *y w ; Sec16.sGFP$^{fTRG.1259}$* (318329; Vienna *Drosophila* Resource Center); *w ; Tango1^{GS15095}/CyO* (206-078; *Drosophila* Genomics and Genetics Resources); *w ; FRT40A* (gift from T. Xu, Yale University School of Medicine, New Haven, CT); *w ; FRT40A Tango1^{GS15095}/CyO* (recombined in this study); *y w ey-Flp* (5580; Bloomington *Drosophila* Stock Center); *y w ey-Flp ; FRT40A tub-GAL80 ; act-y^{+}-GAL4 UAS-GFP* (gift from T. Xu); *w ; FRT82B y w ; FRT82B Sar1$^{11-3-63}$/TM6B* (53710; Bloomington *Drosophila* Stock Center); *w Pxn.B-Flp.F12a* (this study); *w Pxn.B-Flp.F12a ; FRT40A tub-GAL80 ; act-y^{+}-GAL4 UAS-GFP; w ; UAS-YFP.Rab1* (24104; Bloomington *Drosophila* Stock Center); *w ; UAS-Tango1.HA.3.1* (this study); *w ; UAS-Tango1.FLAG.3.1* (this study); *w ; UAS-GFP.Tango1^{CYT}.3.1* (this study); *w ; UAS-Tango1.attP2* (this study); *w ; UAS-SP.GFP.Tango1.3.1* (this study); *y w; Sar1^{CA07674}.GFP/TM3, Ser Sb* (51180; Bloomington *Drosophila* Stock Center).

Constructs

UAS-SP^{Vkg}.RFP and UAS-SP^{Cg25C}.RFP. SignalP 4.1 (Petersen et al., 2011) was used to predict signal peptide cleavage positions in Cg25C and Vkg. Fragments encoding the 23 first amino acids of Cg25C and 30 first amino acids of Vkg were PCR-amplified from pDONR221-Cg25C (Zang et al., 2015) and pDONR221-vkg (see last paragraph in this same section) with primers adding att sites at the 5′ and 3′ termini of the ORF for subsequent Gateway cloning. Primers were attSPCg25C-F: 5′-GGGGACAAGTTTGTACAAAAAAGCAGGCTTCATGTTGCCCTTCTGGAAGCGGCT-3′; attSPCg25C-R: 5′-GGGGACCACTTTGTACAAGAAAGCTGGGTCAGCGTCGGCACCGACTAACGCTC-3′; attSPVkg-F: 5′-GGGGACAAGTTTGTACAAAAAAGCAGGCTTCATGTTACCCAGAGATCTAAGGCA-3′; and attSPVkg-R: 5′-GGGGACCACTTTGTACAAGAAAGCTGGGTCTCCATCCGCCAAGGTAACGGAA-3′.

Fragments thus obtained were purified by gel extraction using AxyPrep DNA Gel Extraction kit (cat#AP-GX-250G; Axygen) and cloned into vector pDONR221 (cat#12536017; Thermo Fisher Scientific) with Gateway BP Clonase Enzyme Mix (cat#11789020; Thermo Fisher Scientific) to obtain entry clones pDONR221-SP^{Cg25C} and pDONR221-Sp^{Vkg}. From these entry clones, SP^{Cg25C} and SP^{Vkg} sequences were transferred into destination vector pTWR (UAST C-terminal RFP, *Drosophila* Carnegie Vector collection) using Gateway LR Clonase Enzyme Mix (cat#12538120; Thermo Fisher Scientific).

pDONR221-Vkg was obtained by PCR-amplifying the coding sequence of *vkg* from L3 larval cDNA synthesized using PrimeScript RT-PCR kit (cat#RR014-A; Takara Bio Inc.). Primers used were attVkg-F: 5′-GGGGACAAGTTTGTACAAAAAAGCAGGCTTCATGTTACCCAGAGATCTAAGGC-3′ and attVkg-R: 5′-GGGGACCACTTTGTACAAGAAAGCTGGGTCGGGGGCGGTGGTGTCCTCGC-3′. The resulting fragment was purified through gel extraction and cloned into pDONR221 through Gateway recombination.

UAS-LanB1.RFP. The coding sequence of *LanB1*, encoding *Drosophila* Laminin β chain, was amplified by PCR from whole L3 larva cDNA using primers attLanB1-F: 5′-GGGGACAAGTTTGTACAAAAAAGCAGGCTTCATGTTGGAGCTGCGGCTT-3′ and attLanB1-R: 5′-GGGGACCACTTTGTACAAGAAAGCTGGGTCCGTATAGCACTGCCTGTA. This fragment was cloned into plasmid pDONR221 to obtain pDONR221-LanB1 and from there transferred to pTWR (UAST C-terminal RFP, *Drosophila* Carnegie Vector collection) using Gateway recombination.

Pxn.B-Flp. To generate hemocyte-specific flippase, a 1.6-kb fragment of the *Pxn* promoter was amplified from genomic DNA with the following att primers: attPxnB-F: 5′-GGGGACAAGTTTGTACAAAAAAGCAGGCTCAGCAAAGCGGAGAAATTTTA-3′ and attPxnB-R: 5′-GGGGACCACTTTGTACAAGAAAGCTGGGTCTACGAGGGCAGTCTAGTTTCG-3′. This fragment was cloned into plasmid pDONR201 to obtain pDONR201-Pxn.B and from there transferred to destination vector pCaSpeR-DEST5 (*Drosophila* Genomics Resource Center) using Gateway recombination.

UAS-Tango1, Tango1.GFP, Tango1.FLAG, and Tango1.HA. The coding sequence of *Tango1* was amplified by PCR from cDNA clone GH02877 (*Drosophila* Genomics Resource Center) using primers attTango1-NF: 5′-GGGGACAAGTTTGTACAAAAAAGCAGGCTTCATGCGGCTGACCAACGAGAA-3′ and attTango1-CF: 5′-GGGGACCACTTTGTACAAGAAAGCTGGGTCTACCTCGCTGTAGGGTCGCG-3′. This fragment was purified through gel extraction, cloned into pDONR221 to obtain pDONR221-Tango1 and from there transferred to destination vector pVALIUM10-roe (UAS site-specific genome integration, gift from J.-Q. Ni (Tsinghua University, Beijing, China) by Gateway LR reaction.

In the same way, pDONR221-Tango1 was recombined with pTWG (UAST C-terminal GFP, *Drosophila* Carnegie Vector collection), pTWF (UAST C-terminal FLAG, *Drosophila* Carnegie Vector collection) and pTWH (UAST C-terminal HA, *Drosophila* Carnegie Vector collection).

UAS-Tango1$^{\Delta CYT}$.GFP. Deletion of the cytoplasmic part of Tango1 was achieved by PCR-amplifying plasmid pTWG-Tango1 with primers Tango1DCYT-F: 5′-TACTACTGCTTCGACCCAGCTTTCTTGTACAAAGTGGTGAGCTCCGCCACC-3′ and Tango1DCYT-R: 5′-GCTGGGTCGAAGCAGTAGTATGCAAACATGAAGAACAAGGAAGAAATC-3′. The resulting PCR product was incubated with DMT enzyme (cat#GD111-01; Transgen Biotech) and transformed into DMT competent cells (cat#CD511-01; Transgen Biotech).

UAS-GFP.Tango1^{CYT}, ^{CC}, ^{CCa}, ^{CCb}, ^{CCc}, ^{CCd}, and $^{Pro\text{-}rich}$. Sequences encoding the cytoplasmic portion of Tango1 or parts of it were amplified from pDONR-Tango1 with the following primers: attTango1CYT-F: 5′-GGGGACAAGTTTGTACAAAAAAGCAGGCTTCTGCAATAGTAGTCAGGAGGG-3′; attTango1CYT-R: 5′-GGGGACCACTTTGTACAAGAAAGCTGGGTCTACCTCGCTGTAGGGTCGCG-3′; attTango1CC-F (=CCa-F): 5′-GGGGACAAGTTTGTACAAAAAAGCAGGCTTCTCAAACGACATGGTGGCCGATCTC-3′; attTango1CC-R (=CCb-R): 5′-GGGGACCACTTTGTACAAGAAAGCTGGGTCGGCCATTGTGGTCAGCTTAC-3′; attTango1CCa-R: 5′-GGGGACCACTTTGTACAAGAAAGCTGGGTCCTTCATCAGCGTCTGGGTCTCAAC-3′; attTango1CCb-F: 5′-GGGGACAAGTTTGTACAAAAAAGCAGGCTTCAACGAAATCCAAACTCTGAAATCTC-3′; attTango1Pro-F: 5′-GGGGACAAGTTTGTACAAAAAAGCAGGCTTCAGCGGCGGAGGAGGAGTAGG-3′; attTango1Pro-R: 5′-GGGGACCACTTTGTACAAGAAAGCTGGGTCTACCTCGCTGTAGGGTCGCGAT-3′; attTango1CCc-F: 5′-GGGGACAAGTTTGTACAAAAAAGCAGGCTTCGTGGCCGATCTCAAGAAGCAA-3′; attTango1CCc-R: 5′-GGGGACCACTTTGTACAAGAAAGCTGGGTCGACTGCCTTCAGGCAATCTTC-3′; attTango1CCd-F: 5′-GGGGACAAGTTTGTACAAAAAAGCAGGCTTCAAGACACGCGGTGAACTCAAC-3′; attTango1CCd-R: 5′-GGGGACCACTTTGTACAAGAAAGCTGGGTCGGTCAGCTTACGCCTCAGGCT-3′. Fragments thus obtained were purified through gel extraction, cloned into pDONR221 and from there transferred into pTGW (UAST N-terminal GFP, *Drosophila* Carnegie Vector collection).

UAS-SP.GFP.Tango1. To express Tango1 N-terminally tagged with GFP after its signal peptide, we modified pTGW (UAST N-terminal GFP, *Drosophila* Carnegie Vector collection) by adding the signal peptide of Tango1 5′ to the GFP sequence as well as SpeI and XhoI restriction sites 3′ to the GFP sequence. To do this, the GFP sequence was PCR-amplified from pTGW with primers adding att sites and restriction sites for NheI (5′) and XhoI followed by SpeI (3′) as follows: attNheIGFP-F: 5′-GGGGACAAGTTTGTACAAAAAAGCAGGCTCTAGCTAGCATGGTGAGCAAGGGCGAGGA-3′; attXhoISpeIGFP-R: 5′-GGGGACCACTTTGTACAAGAAAGCTGGGTCTCGAGCGGGACTAGTCTTGTACAGCTCGTCCATGC-3′.

The resulting fragment was cloned into pDONR221 and from there transferred into pTGW through Gateway recombination. This produced pTG-NheI-G-XhoI-SpeI-W, which contains two copies of GFP. The original GFP sequence in this plasmid was then excised by double digestion with XbaI (cat#R0145S; New England Biolabs, Inc.), for which a restriction site was already present between the UAS promoter and GFP in the original pTGW, and NheI (cat#R3131L; New England Biolabs, Inc.). The excised GFP sequence was replaced through restriction and ligation with T4 DNA ligase (cat#M0202L; New England Biolabs, Inc.) by the signal peptide of Tango1 (26 first amino acids, predicted by SignalP 4.1), which we PCR-amplified from pDONR221-Tango1 using primers that added the appropriate restriction sites (XbaISP-F: 5′-GGCTCTAGAATGCGGCTGACCAACGAGA-3′ and NheISP-R: 5′-CTAGCTAGCAGCCCACGTCAAAGTTGGAA-3′). We named the resulting plasmid pT-SP-G-XhoI-SpeI-W, which lacks Gateway capabilities. In this vector we finally inserted through restriction and ligation the rest of the Tango1 coding sequence, amplified from pDONR221-Tango1 with primers SpeITango1-F: 5′-GGACTAGTGCGACTCTCTCCGACAAGCG-3′ and XhoITango1-R: 5′-CCGCTCGAGTACCTCGCTGTAGGGTCGCG-3′.

UAS-RFP.Rab1. The coding sequence of *Rab1* was amplified by PCR from whole L3 larva cDNA using primers attRab1-F: 5′-GGGGACAAGTTTGTACAAAAAAGCAGGCTTCATGTCATCTGTGAATCCGGAAT-3′ and attRab1-R: 5′-GGGGACCACTTTGTACAAGAAAGCTGGGTCGCAGCAACCGGATTTGGTGTT-3′. This fragment was cloned into plasmid pDONR221 to obtain pDONR221-Rab1 and from there transferred to pTRW (UAST N-terminal RFP, *Drosophila* Carnegie Vector collection) using Gateway recombination.

act-GAL4. The *actin5C* promoter was PCR-amplified from the pAGW vector (*Drosophila* Carnegie Vector Collection) with primers attActin-F: 5′-GGGGACAAGTTTGTACAAAAAAGCAGGCTGCGCATGCAATTCTATATTCTA-3′ and attActin-R: 5′-GGGGACCACTTTGTACAAGAAAGCTGGGTCATCTGGATCCGGGGTCTCTG-3′. The PCR product was recombined into pDONOR221 vector and transferred into pCaSpeR-DEST6 destination vector (*Drosophila* Genomics Resource Center) using Gateway recombination.

Immunohistochemistry

The following primary antibodies were used: rabbit anti-Cg25C (Zang et al., 2015; 1:5,000), rabbit anti-Ndg (Wolfstetter et al., 2009; 1:2,000), guinea pig anti-Tango1 (Lerner et al., 2013; 1:1,000), rabbit anti-Sec16 (Ivan et al., 2008; 1:1,000), rabbit anti-GM130 (cat#ab30637, 1:500; Abcam), rabbit anti-COPII (Sec23, cat#PA1-069A, 1:500; Thermo Fisher Scientific), and goat anti-Gmap (Riedel et al., 2016; 1:500). Secondary antibodies were IgG conjugated to Alexa Fluor 488, Alexa Fluor 555, or Alexa Fluor 647 (1:200; Thermo Fisher Scientific). Larvae

were predissected in PBS by turning them inside out, fixed in PBS containing 4% PFA, washed in PBS (3 × 10 min), blocked in PBT-BSA (PBS containing 0.1% Triton X-100 detergent, 1% BSA, and 250 mM NaCl), incubated overnight with primary antibody in PBT-BSA in 4°C, washed in PBT-BSA (3 × 20 min), incubated for 2 h with secondary antibody in PBT-BSA at room temperature, and washed in PBT-BSA (3 × 20 min) and PBS (3 × 10 min). Tissues were finally dissected and mounted on a slide with a drop of DAPI-Vectashield (cat#H-1200; Vector Laboratories). For blood cell staining and imaging, blood cells from two to five larvae were bled inside a 20-µl drop of PBS on a glass slide and allowed to attach to the slide for 10 min before fixation.

Imaging

3D-SIM images were acquired at room temperature with a Nikon combined confocal A1/SIM/STORM system equipped with a CFI Apo SR TIRF 100× oil (NA 1.49) objective and an Andor Technology EMCCD camera (iXON DU-897 X-9255). Laser lines at 488, 561 and 640 nm were used for excitation. Stacks of z sections were acquired as follows: Fig. 1 A: 13 images, 0.20-µm step, 2.33-µm range; Fig. 1 B: 21 images, 0.12-µm step, 2.17-µm range; Fig. 1 C: 18 images, 0.24-µm step, 3.95-µm range; Fig. 1 D: 18 images, 0.24-µm step, 2.88-µm range; Fig. 1 E (top): 20 images, 0.24-µm step, 4.40-µm range; and Fig. 1 E (bottom): 21 images, 0.24-µm step, 4.72-µm range. Images shown are maximum intensity projections of two to five consecutive z sections. Reconstruction of SIM images was performed with NIS-Elements AR software (Nikon). Confocal microscopy images were acquired in a ZEISS LSM780 microscope equipped with Plan-Apochromat objectives 20× air (NA 0.8), 40× air (NA 0.95), 63× oil (NA 1.4), and 100× oil (NA 1.4) objectives. For ERES size measurements, images were analyzed with ImageJ and statistical analysis performed with GraphPad Prism. Fluorescent images of larvae were acquired with a Leica Microsystems MZ10F stereomicroscope. Bright-field images of adults and larvae were obtained in a Leica Microsystems M125 stereomicroscope.

Electron microscopy

For transmission electron microscopy, ultrathin sections of larval fat body were obtained following standard procedures. Dissected fat body was fixed in 2.5% glutaraldehyde. Once fixed, fat body was postfixed in 1% osmium tetroxide before embedding in epon. Ultrathin sections were stained in 2% uranyl acetate/lead citrate and imaged in a Hitachi H-7650B microscope.

Immunoprecipitation

Larval fat body was dissected in PBS from 100–200 larvae and homogenized with a motorized pellet pestle in 200 µl ice-cold lysis buffer containing 10 mM Tris-HCl, pH 7.5 (cat#0497-500G; Amresco), 150 mM NaCl (cat#x190; Amresco), 0.5 mM EDTA (cat#60-00-4; Xilonghuagong), 0.5% NP-40 (cat#ZC01468; Loogene), and protease inhibitor (cat#M221-1ML; Amresco). Lysates were cleared by centrifugation (20,000 *g*, 30 min, 4°C) and the supernatant was transferred to a precooled Eppendorf tube. Protein concentration was estimated by BCA assay (cat#SD2006; JK GREEN) with a NanoDrop 2000C. To immunoprecipitate the desired proteins in this study, lysates were incubated with GFP-Trap A beads (also binding YFP; cat#gta-20; ChromoTek), anti-FLAG M2 magnetic beads (cat#M8823-1ML; Sigma-Aldrich), or HA-tag magnetic beads (cat#88838X; Thermo Fisher Scientific) according to the manufacturer's instructions. Proteins bound to beads were eluted before analysis by Western blotting. For GFP beads, 50 µl of 2× SDS sample buffer (120 mM Tris-HCl, pH 6.8, 20% glycerol, 4% SDS [cat#151-21-3; Amresco], 0.04% bromophenol blue, and 10% β-mercaptoethanol [cat#161-0710; Bio-Rad Laboratories]) were added to beads, the mixture was incubated in a heat block at 95°C for 20 min, and GFP beads were separated by centrifugation at 5,000 *g* for 2 min at 4°C. For HA beads, 50 µl nonreducing sample buffer (60 mM Tris-HCl, pH 6.8, 1% SDS, 10% glycerol, and lane marker tracking dye) provided with the kit were added to the beads, the mixture was incubated in a heat block at 95°C for 20 min, HA beads were collected with a magnetic separator, and 2 µl β-mercaptoethanol was added. For FLAG beads, 40 µl of a solution containing 48.5 µl TBS buffer and 1.5 µl of 3× FLAG peptide stock solution (5 µg/µl of 3× FLAG peptide [cat#A6001; ApexBio], 100 mM Tris-HCl, pH 7.5, and 200 mM NaCl) were added to beads (150 ng/µl of 3× FLAG final concentration), the mixture was incubated in a rotator for 1 h at 4°C, FLAG beads were collected with a magnetic separator, and 10 µl of 5× SDS-PAGE loading buffer (250 mM Tris-HCl, pH 6.8, 50% glycerol, 10% SDS, 0.5% bromophenol blue, and 5% β-mercaptoethanol) was added to the sample.

Western blotting

For Western blotting, the eluted protein samples were reduced by boiling 5 min at 95°C, separated (25 µl per lane) through SDS-PAGE in a 4–20% gradient gel (MiniProtean TGX; cat#456-1093; Bio-Rad Laboratories), and then electrophoretically transferred onto a nitrocellulose membrane (cat#1620115; Bio-Rad Laboratories) using a wet transfer system (cat#1658034; Bio-Rad Laboratories). The membranes were blocked with 10% milk (cat#LP0031; Oxoid) in TBST (Tris-buffered saline and 0.1% Tween 20), incubated with the primary antibody overnight, washed with TBST (4 × 10 min), incubated with HRP-coupled secondary antibody (1:10,000, 1 h), and washed with TBST (4 × 10 min) again. Secondary antibodies were detected through autoradiography using ECL Plus chemiluminescence (cat#32132; Thermo Fisher Scientific). Primary antibodies were anti-GFP (recognizing also YFP, mouse, CMCTAG, cat#AT0028, 1:5,000), anti-Tango1 (guinea pig, 1:5,000), anti-GM130 (rabbit, cat#ab30637, 1:1,000; Abcam), anti-FLAG (mouse, cat#RLM3001, 1:2,500; Ruiying Biological), and anti-HA (mouse, cat#RLM3003, 1:2,500; Ruiying Biological). The secondary antibodies were HRP-coupled anti–mouse (cat#M21001L; Abmart), anti–rabbit (cat#M21002L; Abmart), and anti–guinea pig (cat#ab6908; Abcam), all at 1:2,000 dilution. Precision Plus Protein Dual Color Standards (cat#161-0394; Bio-Rad Laboratories) was used as a molecular weight marker.

S2 cell transfection

Drosophila S2 cells were grown in Schneider's *Drosophila* Medium (cat#21720024; Thermo Fisher Scientific, Gibco) with 10% FBS premium (cat#P30-3302; PAN Biotech) and 1× antibiotic-antimycotic (cat#15240062; Thermo Fisher Scientific, Gibco) at 28°C. Transfections were performed in 24-well plates. 6 h before transfection, 500 µl of cell culture was added to each well and a round coverslip placed inside. For each transfection, 250 ng act-GAL4 plasmid, 250 ng of the appropriate UAS plasmid, and 1 µl Chemifect transfection reagent (cat#FR-01; Fengruibiology) were incubated together in 100 µl Schneider medium for 30 min at room temperature in an Eppendorf tube before being added to the well containing the cells. After 24 h, coverslips inside wells were taken out with attached cells, washed with PBS (2 × 5 min), fixed in PBS containing 4% PFA for 10 min, and washed again with PBS (2 × 5 min). For antibody staining, cells attached to coverslips were blocked in PBT-BSA (3 × 10 min), incubated for 2 h with primary antibody in PBT-BSA at 4°C, washed with PBT-BSA (3 × 10 min), incubated for 1 h with secondary antibody at room temperature, washed with PBT-BSA (3 × 10 min), and washed with PBS (2 × 5 min). Finally, the coverslips were mounted with DAPI-Vectashield on a slide.

Online supplemental material

Fig. S1 documents the efficiency of Tango1 knockdown. Fig. S2 shows that overexpression of Collagen IV or Laminin single chains does not

impair general secretion. Fig. S3 presents an analysis of Tango1 mutant mosaics. Fig. S4 shows validation of anti-Rab1 antibody. Table S1 lists the predicted molecular weights of secreted proteins in this study. Table S2 quantifies rescue of Tango1 knockdown by cytoplasmic Tango1. Table S3 lists all experimental genotypes.

Acknowledgments

We thank Hugo Bellen (*BM-40-SPARC-GAL4*), Fujian Zhang (*UAS-secr.GFP*), Thomas Lecuit (*Ub-VSVG.GFP*), Isabel Guerrero (*hh-GAL4* and *UAS-hh.GFP*), Sally Horne-Badovinac (anti-Tango1), Stefan Baumgartner (anti-Ndg), Catherine Rabouille (anti-Sec16), Sean Munro (anti-Gmap), the Developmental Studies Hybridoma Bank, the Bloomington *Drosophila* Stock Center, the Kyoto Stock Center, the Vienna *Drosophila* RNAi Center, the Tsinghua Fly Center, the *Drosophila* Genomics Research Center (Indiana), and the *Drosophila* Carnegie Vector Collection for providing fly strains, antibodies, and plasmids. We also thank Yiran Zang and Wenxue Gu, as well as the Tsinghua Electron Microscopy (Lihong Cui and Ying Li) and Imaging (Xuan Tang) facilities, for assistance and Vivek Malhotra for discussion of results and views before publication.

This work was supported by grants from the National Science Foundation of China (31371459 and 31550110204) and the Tsinghua University Initiative Program (20131089281) and by a 1000 Talents award (all to J.C. Pastor-Pareja).

The authors declare no competing financial interests.

Author contributions: M. Liu, Z. Feng, H. Ke, Y. Liu, T. Sun, J. Dai, W. Cui, and J.C. Pastor-Pareja designed experiments, performed experiments, and analyzed the data. J.C. Pastor-Pareja wrote the manuscript.

Submitted: 16 November 2016
Revised: 10 January 2017
Accepted: 11 January 2017

References

Abrams, E.W., and D.J. Andrew. 2005. CrebA regulates secretory activity in the *Drosophila* salivary gland and epidermis. *Development.* 132:2743–2758. http://dx.doi.org/10.1242/dev.01863

Bannykh, S.I., T. Rowe, and W.E. Balch. 1996. The organization of endoplasmic reticulum export complexes. *J. Cell Biol.* 135:19–35. http://dx.doi.org/10.1083/jcb.135.1.19

Bard, F., L. Casano, A. Mallabiabarrena, E. Wallace, K. Saito, H. Kitayama, G. Guizzunti, Y. Hu, F. Wendler, R. Dasgupta, et al. 2006. Functional genomics reveals genes involved in protein secretion and Golgi organization. *Nature.* 439:604–607. http://dx.doi.org/10.1038/nature04377

Bharucha, N., Y. Liu, E. Papanikou, C. McMahon, M. Esaki, P.D. Jeffrey, F.M. Hughson, and B.S. Glick. 2013. Sec16 influences transitional ER sites by regulating rather than organizing COPII. *Mol. Biol. Cell.* 24:3406–3419. http://dx.doi.org/10.1091/mbc.E13-04-0185

Bonifacino, J.S., and B.S. Glick. 2004. The mechanisms of vesicle budding and fusion. *Cell.* 116:153–166. http://dx.doi.org/10.1016/S0092-8674(03)01079-1

Boyadjiev, S.A., J.C. Fromme, J. Ben, S.S. Chong, C. Nauta, D.J. Hur, G. Zhang, S. Hamamoto, R. Schekman, M. Ravazzola, et al. 2006. Cranio-lenticulo-sutural dysplasia is caused by a SEC23A mutation leading to abnormal endoplasmic-reticulum-to-Golgi trafficking. *Nat. Genet.* 38:1192–1197. http://dx.doi.org/10.1038/ng1876

Brand, A.H., and N. Perrimon. 1993. Targeted gene expression as a means of altering cell fates and generating dominant phenotypes. *Development.* 118:401–415.

Brandizzi, F., and C. Barlowe. 2013. Organization of the ER-Golgi interface for membrane traffic control. *Nat. Rev. Mol. Cell Biol.* 14:382–392. http://dx.doi.org/10.1038/nrm3588

Canty, E.G., and K.E. Kadler. 2005. Procollagen trafficking, processing and fibrillogenesis. *J. Cell Sci.* 118:1341–1353. http://dx.doi.org/10.1242/jcs.01731

daSilva, L.L., E.L. Snapp, J. Denecke, J. Lippincott-Schwartz, C. Hawes, and F. Brandizzi. 2004. Endoplasmic reticulum export sites and Golgi bodies behave as single mobile secretory units in plant cells. *Plant Cell.* 16:1753–1771. http://dx.doi.org/10.1105/tpc.022673

Erives, A.J. 2015. Genes conserved in bilaterians but jointly lost with Myc during nematode evolution are enriched in cell proliferation and cell migration functions. *Dev. Genes Evol.* 225:259–273. http://dx.doi.org/10.1007/s00427-015-0508-1

Fessler, J.H., and L.I. Fessler. 1989. *Drosophila* extracellular matrix. *Annu. Rev. Cell Biol.* 5:309–339. http://dx.doi.org/10.1146/annurev.cb.05.110189.001521

Fromme, J.C., and R. Schekman. 2005. COPII-coated vesicles: Flexible enough for large cargo? *Curr. Opin. Cell Biol.* 17:345–352. http://dx.doi.org/10.1016/j.ceb.2005.06.004

Gillingham, A.K., and S. Munro. 2016. Finding the Golgi: Golgin coiled-coil proteins show the way. *Trends Cell Biol.* 26:399–408. http://dx.doi.org/10.1016/j.tcb.2016.02.005

Glick, B.S., and A. Nakano. 2009. Membrane traffic within the Golgi apparatus. *Annu. Rev. Cell Dev. Biol.* 25:113–132. http://dx.doi.org/10.1146/annurev.cellbio.24.110707.175421

Groth, A.C., M. Fish, R. Nusse, and M.P. Calos. 2004. Construction of transgenic *Drosophila* by using the site-specific integrase from phage phiC31. *Genetics.* 166:1775–1782. http://dx.doi.org/10.1534/genetics.166.4.1775

Hynes, R.O., and Q. Zhao. 2000. The evolution of cell adhesion. *J. Cell Biol.* 150:F89–F96. http://dx.doi.org/10.1083/jcb.150.2.F89

Ishikawa, Y., S. Ito, K. Nagata, L.Y. Sakai, and H.P. Bächinger. 2016. Intracellular mechanisms of molecular recognition and sorting for transport of large extracellular matrix molecules. *Proc. Natl. Acad. Sci. USA.* 113:E6036–E6044. http://dx.doi.org/10.1073/pnas.1609571113

Ivan, V., G. de Voer, D. Xanthakis, K.M. Spoorendonk, V. Kondylis, and C. Rabouille. 2008. *Drosophila* Sec16 mediates the biogenesis of tER sites upstream of Sar1 through an arginine-rich motif. *Mol. Biol. Cell.* 19:4352–4365. http://dx.doi.org/10.1091/mbc.E08-03-0246

Jensen, D., and R. Schekman. 2011. COPII-mediated vesicle formation at a glance. *J. Cell Sci.* 124:1–4. http://dx.doi.org/10.1242/jcs.069773

Jin, L., K.B. Pahuja, K.E. Wickliffe, A. Gorur, C. Baumgärtel, R. Schekman, and M. Rape. 2012. Ubiquitin-dependent regulation of COPII coat size and function. *Nature.* 482:495–500. http://dx.doi.org/10.1038/nature10822

Johnson, A., N. Bhattacharya, M. Hanna, J.G. Pennington, A.L. Schuh, L. Wang, M.S. Otegui, S.M. Stagg, and A. Audhya. 2015. TFG clusters COP II-coated transport carriers and promotes early secretory pathway organization. *EMBO J.* 34:811–827. http://dx.doi.org/10.15252/embj.201489032

Kelley, L.C., L.L. Lohmer, E.J. Hagedorn, and D.R. Sherwood. 2014. Traversing the basement membrane in vivo: A diversity of strategies. *J. Cell Biol.* 204:291–302. http://dx.doi.org/10.1083/jcb.201311112

Kondylis, V., and C. Rabouille. 2009. The Golgi apparatus: Lessons from *Drosophila*. *FEBS Lett.* 583:3827–3838. http://dx.doi.org/10.1016/j.febslet.2009.09.048

Kramer, J.M. 1994. Genetic analysis of extracellular matrix in *C. elegans*. *Annu. Rev. Genet.* 28:95–116. http://dx.doi.org/10.1146/annurev.ge.28.120194.000523

Kumichel, A., K. Kapp, and E. Knust. 2015. A conserved di-basic motif of *Drosophila* Crumbs contributes to efficient ER export. *Traffic.* 16:604–616. http://dx.doi.org/10.1111/tra.12273

Kurokawa, K., M. Okamoto, and A. Nakano. 2014. Contact of cis-Golgi with ER exit sites executes cargo capture and delivery from the ER. *Nat. Commun.* 5:3653. http://dx.doi.org/10.1038/ncomms4653

Lee, T., and L. Luo. 2001. Mosaic analysis with a repressible cell marker (MARCM) for *Drosophila* neural development. *Trends Neurosci.* 24:251–254. http://dx.doi.org/10.1016/S0166-2236(00)01791-4

Lerner, D.W., D. McCoy, A.J. Isabella, A.P. Mahowald, G.F. Gerlach, T.A. Chaudhry, and S. Horne-Badovinac. 2013. A Rab10-dependent mechanism for polarized basement membrane secretion during organ morphogenesis. *Dev. Cell.* 24:159–168. http://dx.doi.org/10.1016/j.devcel.2012.12.005

Lunstrum, G.P., H.P. Bächinger, L.I. Fessler, K.G. Duncan, R.E. Nelson, and J.H. Fessler. 1988. *Drosophila* basement membrane procollagen IV. I. Protein characterization and distribution. *J. Biol. Chem.* 263:18318–18327.

Maeda, M., K. Saito, and T. Katada. 2016. Distinct isoform-specific complexes of TANGO1 cooperatively facilitate collagen secretion from the

endoplasmic reticulum. *Mol. Biol. Cell.* 27:2688–2696. http://dx.doi.org/10.1091/mbc.E16-03-0196

Malhotra, V., and P. Erlmann. 2011. Protein export at the ER: Loading big collagens into COPII carriers. *EMBO J.* 30:3475–3480. http://dx.doi.org/10.1038/emboj.2011.255

Malhotra, V., and P. Erlmann. 2015. The pathway of collagen secretion. *Annu. Rev. Cell Dev. Biol.* 31:109–124. http://dx.doi.org/10.1146/annurev-cellbio-100913-013002

McCaughey, J., V.J. Miller, N.L. Stevenson, A.K. Brown, A. Budnik, K.J. Heesom, D. Alibhai, and D.J. Stephens. 2016. tfg promotes organization of transitional ER and efficient collagen secretion. *Cell Reports.* 15:1648–1659. http://dx.doi.org/10.1016/j.celrep.2016.04.062

Meyer, F., and B. Moussian. 2009. *Drosophila* multiplexin (Dmp) modulates motor axon pathfinding accuracy. *Dev. Growth Differ.* 51:483–498. http://dx.doi.org/10.1111/j.1440-169X.2009.01111.x

Miller, E.A., and R. Schekman. 2013. COPII - A flexible vesicle formation system. *Curr. Opin. Cell Biol.* 25:420–427. http://dx.doi.org/10.1016/j.ceb.2013.04.005

Natzle, J.E., J.M. Monson, and B.J. McCarthy. 1982. Cytogenetic location and expression of collagen-like genes in *Drosophila*. *Nature.* 296:368–371. http://dx.doi.org/10.1038/296368a0

Nogueira, C., P. Erlmann, J. Villeneuve, A.J. Santos, E. Martínez-Alonso, J.A. Martínez-Menárguez, and V. Malhotra. 2014. SLY1 and Syntaxin 18 specify a distinct pathway for procollagen VII export from the endoplasmic reticulum. *eLife.* 3:e02784. http://dx.doi.org/10.7554/eLife.02784

Pastor-Pareja, J.C., and T. Xu. 2011. Shaping cells and organs in *Drosophila* by opposing roles of fat body-secreted Collagen IV and perlecan. *Dev. Cell.* 21:245–256. http://dx.doi.org/10.1016/j.devcel.2011.06.026

Petersen, T.N., S. Brunak, G. von Heijne, and H. Nielsen. 2011. SignalP 4.0: Discriminating signal peptides from transmembrane regions. *Nat. Methods.* 8:785–786. http://dx.doi.org/10.1038/nmeth.1701

Petley-Ragan, L.M., E.L. Ardiel, C.H. Rankin, and V.J. Auld. 2016. Accumulation of laminin monomers in *Drosophila* glia leads to glial endoplasmic reticulum stress and disrupted larval locomotion. *J. Neurosci.* 36:1151–1164. http://dx.doi.org/10.1523/JNEUROSCI.1797-15.2016

Raote, I., M. Ortega Bellido, M. Pirozzi, C. Zhang, D. Melville, S. Parashuraman, T. Zimmermann, and V. Malhotra. 2017. TANGO1 assembles into rings around COPII coats at ER exit sites. *J. Cell Biol.* 216. http://dx.doi.org/10.1083/jcb.201608080

Riedel, F., A.K. Gillingham, C. Rosa-Ferreira, A. Galindo, and S. Munro. 2016. An antibody toolkit for the study of membrane traffic in *Drosophila melanogaster*. *Biol. Open.* 5:987–992. http://dx.doi.org/10.1242/bio.018937

Ripoche, J., B. Link, J.K. Yucel, K. Tokuyasu, and V. Malhotra. 1994. Location of Golgi membranes with reference to dividing nuclei in syncytial *Drosophila* embryos. *Proc. Natl. Acad. Sci. USA.* 91:1878–1882. http://dx.doi.org/10.1073/pnas.91.5.1878

Roote, J., and A. Prokop. 2013. How to design a genetic mating scheme: A basic training package for *Drosophila* genetics. *G3 (Bethesda).* 3:353–358. http://dx.doi.org/10.1534/g3.112.004820

Rubin, G.M., and A.C. Spradling. 1982. Genetic transformation of *Drosophila* with transposable element vectors. *Science.* 218:348–353. http://dx.doi.org/10.1126/science.6289436

Saito, K., M. Chen, F. Bard, S. Chen, H. Zhou, D. Woodley, R. Polischuk, R. Schekman, and V. Malhotra. 2009. TANGO1 facilitates cargo loading at endoplasmic reticulum exit sites. *Cell.* 136:891–902. http://dx.doi.org/10.1016/j.cell.2008.12.025

Saito, K., K. Yamashiro, Y. Ichikawa, P. Erlmann, K. Kontani, V. Malhotra, and T. Katada. 2011. cTAGE5 mediates collagen secretion through interaction with TANGO1 at endoplasmic reticulum exit sites. *Mol. Biol. Cell.* 22:2301–2308. http://dx.doi.org/10.1091/mbc.E11-02-0143

Saito, K., K. Yamashiro, N. Shimazu, T. Tanabe, K. Kontani, and T. Katada. 2014. Concentration of Sec12 at ER exit sites via interaction with cTAGE5 is required for collagen export. *J. Cell Biol.* 206:751–762. http://dx.doi.org/10.1083/jcb.201312062

Santos, A.J., I. Raote, M. Scarpa, N. Brouwers, and V. Malhotra. 2015. TANGO1 recruits ERGIC membranes to the endoplasmic reticulum for procollagen export. *eLife.* 4:e10982. http://dx.doi.org/10.7554/eLife.10982

Santos, A.J., C. Nogueira, M. Ortega-Bellido, and V. Malhotra. 2016. TANGO1 and Mia2/cTAGE5 (TALI) cooperate to export bulky pre-chylomicrons/VLDLs from the endoplasmic reticulum. *J. Cell Biol.* 213:343–354. http://dx.doi.org/10.1083/jcb.201603072

Sparkes, I.A., T. Ketelaar, N.C. de Ruijter, and C. Hawes. 2009. Grab a Golgi: Laser trapping of Golgi bodies reveals in vivo interactions with the endoplasmic reticulum. *Traffic.* 10:567–571. http://dx.doi.org/10.1111/j.1600-0854.2009.00891.x

Tanabe, T., M. Maeda, K. Saito, and T. Katada. 2016. Dual function of cTAGE5 in collagen export from the endoplasmic reticulum. *Mol. Biol. Cell.* 27:2008–2013. http://dx.doi.org/10.1091/mbc.E16-03-0180

Tisdale, E.J., J.R. Bourne, R. Khosravi-Far, C.J. Der, and W.E. Balch. 1992. GTP-binding mutants of rab1 and rab2 are potent inhibitors of vesicular transport from the endoplasmic reticulum to the Golgi complex. *J. Cell Biol.* 119:749–761. http://dx.doi.org/10.1083/jcb.119.4.749

Tiwari, P., A. Kumar, R.N. Das, V. Malhotra, and K. VijayRaghavan. 2015. A tendon cell specific RNAi screen reveals novel candidates essential for muscle tendon interaction. *PLoS One.* 10:e0140976. http://dx.doi.org/10.1371/journal.pone.0140976

Tsarouhas, V., K.A. Senti, S.A. Jayaram, K. Tiklová, J. Hemphälä, J. Adler, and C. Samakovlis. 2007. Sequential pulses of apical epithelial secretion and endocytosis drive airway maturation in *Drosophila*. *Dev. Cell.* 13:214–225. http://dx.doi.org/10.1016/j.devcel.2007.06.008

Usener, D., D. Schadendorf, J. Koch, S. Dübel, and S. Eichmüller. 2003. cTAGE: A cutaneous T cell lymphoma associated antigen family with tumor-specific splicing. *J. Invest. Dermatol.* 121:198–206. http://dx.doi.org/10.1046/j.1523-1747.2003.12318.x

Venditti, R., T. Scanu, M. Santoro, G. Di Tullio, A. Spaar, R. Gaibisso, G.V. Beznoussenko, A.A. Mironov, A. Mironov Jr., L. Zelante, et al. 2012. Sedlin controls the ER export of procollagen by regulating the Sar1 cycle. *Science.* 337:1668–1672. http://dx.doi.org/10.1126/science.1224947

Wendler, F., A.K. Gillingham, R. Sinka, C. Rosa-Ferreira, D.E. Gordon, X. Franch-Marro, A.A. Peden, J.P. Vincent, and S. Munro. 2010. A genome-wide RNA interference screen identifies two novel components of the metazoan secretory pathway. *EMBO J.* 29:304–314. http://dx.doi.org/10.1038/emboj.2009.350

Wilkin, M.B., M.N. Becker, D. Mulvey, I. Phan, A. Chao, K. Cooper, H.J. Chung, I.D. Campbell, M. Baron, and R. MacIntyre. 2000. *Drosophila* dumpy is a gigantic extracellular protein required to maintain tension at epidermal-cuticle attachment sites. *Curr. Biol.* 10:559–567. http://dx.doi.org/10.1016/S0960-9822(00)00482-6

Wilson, D.G., K. Phamluong, L. Li, M. Sun, T.C. Cao, P.S. Liu, Z. Modrusan, W.N. Sandoval, L. Rangell, R.A. Carano, et al. 2011. Global defects in collagen secretion in a Mia3/TANGO1 knockout mouse. *J. Cell Biol.* 193:935–951. (published erratum appears in *J. Cell Biol.* 2011. 194:347) http://dx.doi.org/10.1083/jcb.201007162

Witte, K., A.L. Schuh, J. Hegermann, A. Sarkeshik, J.R. Mayers, K. Schwarze, J.R. Yates III, S. Eimer, and A. Audhya. 2011. TFG-1 function in protein secretion and oncogenesis. *Nat. Cell Biol.* 13:550–558. http://dx.doi.org/10.1038/ncb2225

Wolfstetter, G., M. Shirinian, C. Stute, C. Grabbe, T. Hummel, S. Baumgartner, R.H. Palmer, and A. Holz. 2009. Fusion of circular and longitudinal muscles in *Drosophila* is independent of the endoderm but further visceral muscle differentiation requires a close contact between mesoderm and endoderm. *Mech. Dev.* 126:721–736. http://dx.doi.org/10.1016/j.mod.2009.05.001

Xu, T., and G.M. Rubin. 1993. Analysis of genetic mosaics in developing and adult *Drosophila* tissues. *Development.* 117:1223–1237.

Yurchenco, P.D. 2011. Basement membranes: Cell scaffoldings and signaling platforms. *Cold Spring Harb. Perspect. Biol.* 3:a004911. http://dx.doi.org/10.1101/cshperspect.a004911

Zang, Y., M. Wan, M. Liu, H. Ke, S. Ma, L.P. Liu, J.Q. Ni, and J.C. Pastor-Pareja. 2015. Plasma membrane overgrowth causes fibrotic collagen accumulation and immune activation in *Drosophila* adipocytes. *eLife.* 4:e07187. http://dx.doi.org/10.7554/eLife.07187

Zhang, L., Z.A. Syed, I. van Dijk Härd, J.-M. Lim, L. Wells, and K.G. Ten Hagen. 2014. O-glycosylation regulates polarized secretion by modulating Tango1 stability. *Proc. Natl. Acad. Sci. USA.* 111:7296–7301. http://dx.doi.org/10.1073/pnas.1322264111